Journal of Renewable Materials

Tech Science Press

Doi:10.32604/jrm.2025.02024-0023 Published Online: 03 March 2025

ARTICLE

Bio-Composite Films from Carrageenan/Starch Reinforced with Nanocellulose for Active Edible Food Packaging: Development and Optimization

Mariia Dmitrenko[1], Daniel Pasquini[2,*], Marcela Piassi Bernardo[2], João Marcelo de Lima Alves[2], Anna Kuzminova[1], Ilnur Dzhakashov[1], Andrey Terentyev[3], Alexander Dyachkov[3], K. S. Joshy[4], Maya Jacob John[5], Sabu Thomas[4] and Anastasia Penkova[1,*]

[1]St. Petersburg State University, 7/9 Universitetskaya nab, St. Petersburg, 199034, Russia
[2]Instituto de Química, Universidade Federal de Uberlândia, Campus Santa Mônica, Av. João Naves de Ávila, 2121, Uberlândia, 38400-902, Minas Gerais, Brazil
[3]Mendeleev University of Chemical Technology of Russia, Miusskaya sq., 9, Moscow, 125047, Russia
[4]International and Inter University Centre for Nanoscience and Nanotechnology, Mahatma Gandhi University, Kottayam, 686560, Kerala, India
[5]Centre for Nanostructures and Advanced Materials, Chemicals Cluster, Council for Scientific and Industrial Research, Pretoria, 0001, South Africa

*Corresponding Authors: Daniel Pasquini. Email: daniel.pasquini@ufu.br; Anastasia Penkova. Email: a.penkova@spbu.ru

Received: 24 October 2024; Accepted: 07 February 2025

ABSTRACT: Petrochemical plastics are widely used for food protection and preservation; however, they exhibit poor biodegradability, resisting natural degradation through physical, chemical, or enzymatic processes. As a sustainable alternative to conventional plastic packaging, edible films offer effective barriers against moisture, gases, and microbial contamination while being biodegradable, biocompatible, and environmentally friendly. In this study, novel active food packaging materials (in film form) were developed by incorporating starch, carrageenan, nanocellulose (NC), *Aloe vera*, and hibiscus flower extract. The effects of varying the matrix composition (26.5–73.5 wt.% starch/carrageenan), NC concentration (2.77–17.07 wt.%), and particle type (fibers or crystals) on the film structure and characteristics were analyzed using various methods. Scanning electron microscopy demonstrated good homogeneity and effective dispersion of NC within the blend matrix. An increased carrageenan content in the film improved wettability, moisture absorption, solubility, and water vapor permeability. The mechanical properties of the films were enhanced by NC incorporation and higher carrageenan content. The developed films also exhibited effective UV radiation barriers and biodegradability. Films with low carrageenan content (less than 33.3%) and high NC content (7%, 10% crystals or 10%, 15% fibers) exhibited optimal properties, including enhanced water resistance, hydrophobicity, and mechanical strength, along with reduced water vapor permeability. However, the high water solubility and moisture absorption (above 55% and 14%, respectively) indicated their unsuitability as packaging materials for food products with wet surfaces and high humidity. The results suggest that these films are well suited for use as edible food packaging for fruits and vegetables.

KEYWORDS: Carrageenan; starch; nanocellulose; edible film; packaging material

1 Introduction

From production in the fields to final consumption, food is vulnerable to external damage, bacterial contamination, and oxidation, all of which can lead to a decline in quality [1]. Petrochemical plastics are extensively used for food protection and preservation. By 2019, global plastic production had surged to 368

million tonnes, with 40% allocated to food packaging and single-use takeaway items [2]. These plastics exhibit poor biodegradability and cannot be effectively broken down by natural physical, chemical, or enzymatic processes. Their accumulation disrupts natural ecosystems and has a profound environmental impact due to their high durability and resistance to degradation, which can persist for up to 400 years [3]. As a result, plastic waste is often disposed of through burial or incineration, contributing to air, water, and soil pollution, and posing risks to human health and the ecological environment [4].

To reduce reliance on conventional plastics, considerable efforts are being made to develop biodegradable materials derived from both synthetic and natural polymers. Edible films, which are thin layers of consumable materials, can act as barriers against moisture, gases, and microbial contamination, thereby extending the shelf life of food products. These films offer a promising alternative to traditional plastic packaging [5]. Furthermore, active packaging technologies can improve the safety and quality of packaged foods by actively modifying the internal environment of the package [6]. From both environmental and economic perspectives, there is an urgent need for bioactive and smart packaging films with antibacterial, antioxidant, and barrier properties, made from biopolymers that are biodegradable, biocompatible, environmentally friendly, and non-toxic [7].

Starch, a naturally abundant, renewable, and biodegradable polysaccharide, emerges as an attractive candidate for replacing traditional plastics in food packaging [8]. Chemically, starch consists of two polysaccharides: amylose and amylopectin. Amylose is a linear polymer with 1,4-glycosidic linkages, while amylopectin is a highly branched polymer with both α-1,4-glycosidic and α-1,6-glycosidic bonds [9]. Starch is valued for its biodegradability, abundance, chemical stability, resistance to degradation, and excellent film-forming properties [10]. At least three components are required to form starch films: starch, a solvent (usually water), and a plasticizer (such as glycerol or sorbitol) [11]. However, starch films often exhibit poor mechanical properties [11]. To address these issues, other biopolymers are commonly added to the film formulation. Additionally, the incorporation of plant extracts and oils can further enhance the films by providing smart and active functions [12].

Carrageenan, a linear polysaccharide derived from red seaweed, consists of galactose and ester sulfates and is known for its excellent film-forming ability [13]. Its addition to starch films has been shown to improve tensile strength [14]. The combination of these polysaccharides can enhance mechanical and functional properties by leveraging the advantages of each component while mitigating their potential limitations [15]. The potential for developing edible films from a carrageenan matrix reinforced with starch granules and nanocellulose was demonstrated in our previous work [16]. However, the novelty of this study lies in the production of films based on a carrageenan/starch polysaccharide blend, where starch granules were destroyed by modifying the preparation conditions at elevated temperatures and incorporating additional agents such as myristic acid (as an effective surfactant for mixing water with oil) and hibiscus flower extract to impart novel properties. Therefore, detailed studies are necessary to understand the mechanisms of interaction affecting film properties.

Cellulose in the form of nanocrystals or nanofibrils can also enhance film properties such as hydrophobicity, thermal stability, barrier characteristics, tensile strength, and elasticity due to its numerous hydroxyl groups, which interact with starch to form a dense network structure [17]. Nanocellulose is classified into two main types: (i) cellulose nanocrystals and (ii) cellulose nanofibrils [18]. Cellulose nanocrystals are rigid, needle-like structures with thicknesses ranging from a few to several tens of nanometers (~3–50 nm) and lengths from tens to hundreds of nanometers (~50–1000 nm). They are typically isolated via acid hydrolysis from delignified and bleached cellulosic fibers. In contrast, cellulose nanofibrils are flexible structures with diameters of tens of nanometers (~5–100 nm) and lengths in the micrometer range (50–3000 nm), obtained by mechanically disrupting bleached cellulose fibers. This disruption is usually achieved through grinding,

high-pressure homogenization, or similar techniques, which subject the fibers to shear forces that separate the microfibrils constituting the fiber cell walls [18]. Due to their distinct properties, various forms of nanocellulose exhibit significant potential as reinforcing agents in composites, leading to different behaviors.

Incorporating antioxidants into edible films can extend shelf life and maintain food quality by gradually releasing these substances into the packaging environment [9]. *Aloe vera*, known for its antimicrobial and antioxidant properties, is widely used in medicine and cosmetics, and it can significantly enhance food packaging by extending the shelf life of perishable products [19]. Raw *Aloe vera* consists of approximately 98% water, with the remaining solid fraction composed of various bioactive compounds, including phenolic compounds, amino acids, enzymes, carbohydrates, lipids, proteins, and vitamins [20]. Its soluble fractions contain mucopolysaccharides, which exhibit bactericidal, fungicidal, and virucidal properties. Several studies have demonstrated the beneficial effects of *Aloe vera* in preventing fruit decay and microbial spoilage [20,21]. *Aloe vera* is an ideal natural antioxidant because it is widely used worldwide, its industrial production process is well established, and it is compatible with various biopolymers. Sesame oil is another natural component that can impart antioxidant properties to edible films [22], while also acting as a plasticizer and compatibilizer, improving the film's hygroscopic properties [23]. Its selection is based on its balanced composition of fatty acids (oleic and linoleic), making it highly beneficial in dietary applications. Sesame oil has been linked to numerous health benefits, including cardiovascular disease prevention, cholesterol regulation, blood sugar control, anti-inflammatory effects, liver protection, and neuroprotective properties, particularly in patients with Alzheimer's disease [24].

Food packaging can also serve as an indicator of food freshness, quality, or safety through sensors and indicators [25]. Color change is a visible and rapid method for assessing food quality, and natural pigments from botanical sources serve as excellent quality indicators [26]. Hibiscus sp. is a herbaceous plant whose calyces are widely used in the food industry for producing herbal infusions, beverages, sauces, juices, jellies, jams, and baked goods [27]. The extract obtained from hibiscus calyces is considered safe as a food additive by the FDA (U.S. Food and Drug Administration) [28]. This extract is rich in bioactive molecules such as anthocyanins, organic acids, alkaloids, phenolic acids, and saponins. Anthocyanins possess antimicrobial and antioxidant properties, making hibiscus extract a valuable addition to food packaging for extending shelf life by acting as a natural preservative. Furthermore, anthocyanins are pH-sensitive pigments, meaning their color changes depending on the surrounding environment [26]. Therefore, incorporating hibiscus extract into film packaging solutions can enable food quality indication—a fundamental feature of smart packaging.

This study presents, for the first time, the development of a smart and active food packaging film composed of starch, carrageenan, nanocellulose, *Aloe vera*, and hibiscus extract. The optimal composition was determined, and the films were thoroughly characterized in terms of structure, morphology, and physicochemical properties.

2 Materials and Methods

2.1 Reagent Extraction

The extraction of carrageenan (gel strength of 170 g/cm^3, ~20% 3,6-anhydrogalactose content, Kottayam, Kerala, India) was carried out from seaweed collected in Trivandrum (Kerala, India). The algal mixture was air-dried at 60°C, boiled in a NaOH solution (1:20 ratio) for 2 h, and filtered into cold ethanol, where the carrageenan precipitated. The precipitate was then filtered, washed with cold ethanol, and dried at 60°C.

To obtain starch (arrowroot, ~30% amylose, Kottayam, Kerala, India), washed and chopped arrowroot rhizomes were placed in a 0.03 wt.% potassium metabisulphite solution for 15 min, followed by grinding

in deionised water with high-speed stirring. The mixture was then filtered through a double layer of cotton cloth, and the resulting homogeneous mass was washed with water to extract the starch. The filtrate was left to stand for 12 h to allow the starch to precipitate. The precipitated starch was dried at 60°C for 5 h and ground in a mixer [29].

A detailed characterization of the polysaccharides obtained using these extraction methods has been published previously [16,29,30].

The preparation of nanocellulose (NC) crystals (particle size with a mean length of 215 ± 52 nm and a mean diameter of 4.9 ± 1.5 nm, Uberlândia, Brazil) was carried out as follows: crushed sheets of eucalyptus kraft bleached pulp (10 g) were immersed in 200 mL of a 60 wt.% sulfuric acid solution in a water bath at 45°C and kept for 55 min under constant mechanical stirring. At the end of the reaction, the dispersion was poured into cold water to stop the reaction and left to settle until the solid particles sank. The solid residue was then placed in a dialysis membrane and washed with water to remove the acid and bring the pH to 7. The suspension was subsequently sonicated to disperse the nanoparticles and obtain the final colloidal dispersion of NC crystals. To determine the NC crystal content, the dispersion was dried in an oven at 50°C for 24 h, and the solid content was calculated based on the mass difference (~2–3 wt.%) [31].

NC fibers (particle size with an average diameter of 10–20 nm and an average length of a few hundred nanometers) were obtained from pineapple leaves collected in Kottayam (Kerala, India). The leaves were cut, oven-dried at 40°C for 24 h, crushed, and treated with 4 wt.% NaOH at 90°C for 2 h to extract lignin and hemicellulose. The next step involved bleaching with 3 wt.% $NaClO_2$ at 90°C, followed by rinsing with 10 wt.% $H_2C_2O_4$ at 120°C under 20 lbs of pressure for 3 h. The resulting NC fibers were thoroughly washed to remove the acid, centrifuged, homogenised, and freeze-dried [32]. To determine the NC fiber content, the dispersion was dried at 50°C, and the solid content was calculated based on the mass difference (~4–5 wt.%).

A detailed characterization of the obtained cellulose nanofibers and nanocrystals has been published previously [16,31].

The extraction of hibiscus flower extract (Uberlândia, Brazil) was carried out as follows: 50 g of crushed dried flowers were placed in 500 mL of water and kept in a water bath at 50°C for 1 h. The solution was then filtered through filter paper to separate the solid residues and transferred to a 500 mL volumetric flask. To determine the solid extract content, a precisely measured mass of the solution was dried at 50°C, and the solid content was calculated based on the mass difference (~3–4 wt.%).

2.2 Materials

Polysaccharides—carrageenan (Kottayam, Kerala, India) and starch (arrowroot, Kottayam, Kerala, India)—in different ratios were used as the film matrix. NC fibers (Kottayam, Kerala, India) and NC crystals (Uberlândia, Brazil) were used as reinforcing agents to improve the mechanical properties of the films. *Aloe vera* gel (Cathedral Pharmaceutical Industry, Brazil) was added to impart antibacterial properties to the films. Sesame oil (Pazze Food Industry, Brazil), myristic acid (≥99%, CAS 544-63-8, Sigma Aldrich, Malaysia), and glycerol (CAS 56-81-5, Dinâmica Company, Brazil) were used as an antioxidant, surfactant, and plasticizer, respectively. $K_2S_2O_5$, $NaClO_2$, and ethanol (Nice Chemicals, India), as well as NaOH flakes and $H_2C_2O_4$ crystals (Sigma-Aldrich, USA), were used in their original forms.

2.3 Preparation of Films

To optimize the composition of the films, different ratios of carrageenan (26.5, 33.3, 50, 66.6, 73.5 wt.%) and starch were tested. The polysaccharide mixture was prepared as follows: the required amounts of carrageenan and starch were combined to obtain 2 g of total polysaccharides. Then, 0.6 g of glycerol was

added, and the mixture was dissolved in 50 mL of water under constant stirring at 500 rpm at 80°C until a homogeneous dispersion was achieved. The temperature of 80°C was chosen to facilitate the dissolution of starch granules. After obtaining a homogeneous dispersion at 80°C, 0.1 g of myristic acid and 0.08 g of sesame oil were added. Sesame oil and glycerol acted as compatibilizers and plasticizers, respectively, to enhance hygroscopic and mechanical properties (brittleness and friability) [16]. Myristic acid served as a surfactant to facilitate the mixing of water and oil, while also functioning as a flavoring agent commonly used in the food industry [33,34]. *Aloe vera* gel (0.1 g) and hibiscus flower extract (1 g) were incorporated to provide antibacterial and functional properties, including color changes in response to pH variations. Finally, NC fibers or crystals were added to enhance the mechanical properties of the films, followed by continuous stirring for 1 h.

To optimize the film composition, the particle structure (fibers or crystals) and NC content were varied. The carrageenan/starch ratio and NC content were adjusted according to the factorial design shown in Table 1. The factorial design matrix for film development is presented in Table 2. In statistical studies using mathematical models, treatments are coded for the levels of variables being tested. These levels are typically referred to as "high" and "low" or "absent" and "present," represented as "+" and "−", or "0" and "1", respectively. However, these codes correspond to actual values of the studied variables/factors [35], as detailed in Table 1. All treatments in the statistical software were conducted using coded level values (−1, 0, +1, etc.), and all equations were generated in coded form. Variations in the concentrations of polysaccharides (carrageenan, starch, and NC) were made while keeping the concentrations of other components constant: 5 wt.% myristic acid, 5 wt.% sesame oil, 30 wt.% glycerol, 5 wt.% *Aloe vera* gel, and 25 wt.% hibiscus flower extract, relative to the mass of the starch/carrageenan matrix. The carrageenan and starch levels were chosen to cover a full range of possible compositions, from high starch and low carrageenan to the reverse. The concentrations of glycerol, *Aloe vera* gel, sesame oil, and myristic acid were selected based on a literature review, ensuring that the chosen amounts provided the desired properties for this study. The hibiscus extract content (25% of the polymer weight) was optimized in a previous study: values below 25% resulted in films with weak coloration, failing to meet the smart packaging requirement of color change with pH variations, whereas values above 25% caused the films to lose transparency and become brittle. Based on previous data, a defined range of NC values above and below the percolation threshold was used to study the behavior of films containing these nanoparticles. Several percolation models exist, including those developed by Takayanagi, Ouali, and the Halpin–Tsai model [36]. These models assume uniform filler dispersion and interaction with the matrix. When a rigid network forms due to strong interactions between filler particles above a critical content, this is referred to as the percolation threshold in the Takayanagi and Ouali model [36]. The range of NC concentrations (2.77–11.23 wt.% for crystals and 2.92–17.07 wt.% for fibers) differed due to structural and crystallinity variations. NC fibers contain both crystalline and amorphous phases, allowing a higher concentration in the polymer matrix compared to NC crystals [37]. At the same NC concentration, crystals are found to be more effective than NC fibers in enhancing the mechanical properties of the composite material.

The films were prepared by depositing nanodispersions onto Petri dishes and evaporating the solvent (water) in an oven without convection at 50°C for 24 h. This temperature was chosen because lower temperatures would prolong the evaporation process, while higher temperatures (above 50°C) would cause film shrinkage and deformation (changes in shape and size).

Photos of the developed films with different polysaccharide compositions (carrageenan, starch, and NC) and their designations in coordinates are shown in Fig. 1. The first coordinate in the film designation represents the carrageenan content, while the second coordinate corresponds to the NC content.

Table 1: The factors and levels used to study the production of nanocomposite films

Factors	Levels				
	$-\sqrt{2}$	−1	0	+1	$+\sqrt{2}$
Carrageenan, wt.%	26.5	33.3	50	66.6	73.5
NC crystals, wt.% with respect to the carrageenan/starch weight	2.77	4	7	10	11.23
NC fibers, wt.% with respect to the carrageenan/starch weight	2.92	5	10	15	17.07

Table 2: The planning matrix for the factorial design used to develop the films

Experiment	Carrageenan, wt.%	NC, wt.%
0 (×2)	0	0
1	−1	−1
2	+1	+1
3	−1	+1
4	+1	−1
5	0	$+\sqrt{2}$
6	0	$-\sqrt{2}$
7	$+\sqrt{2}$	0
8	$-\sqrt{2}$	0

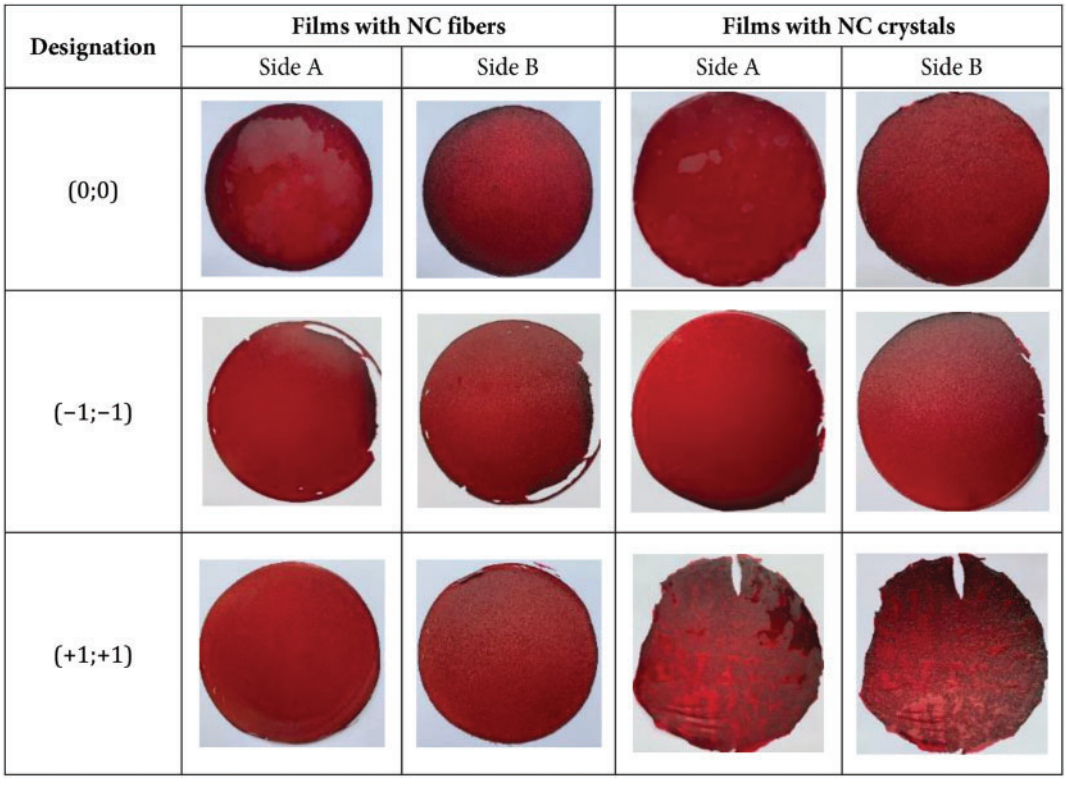

Figure 1: (Continued)

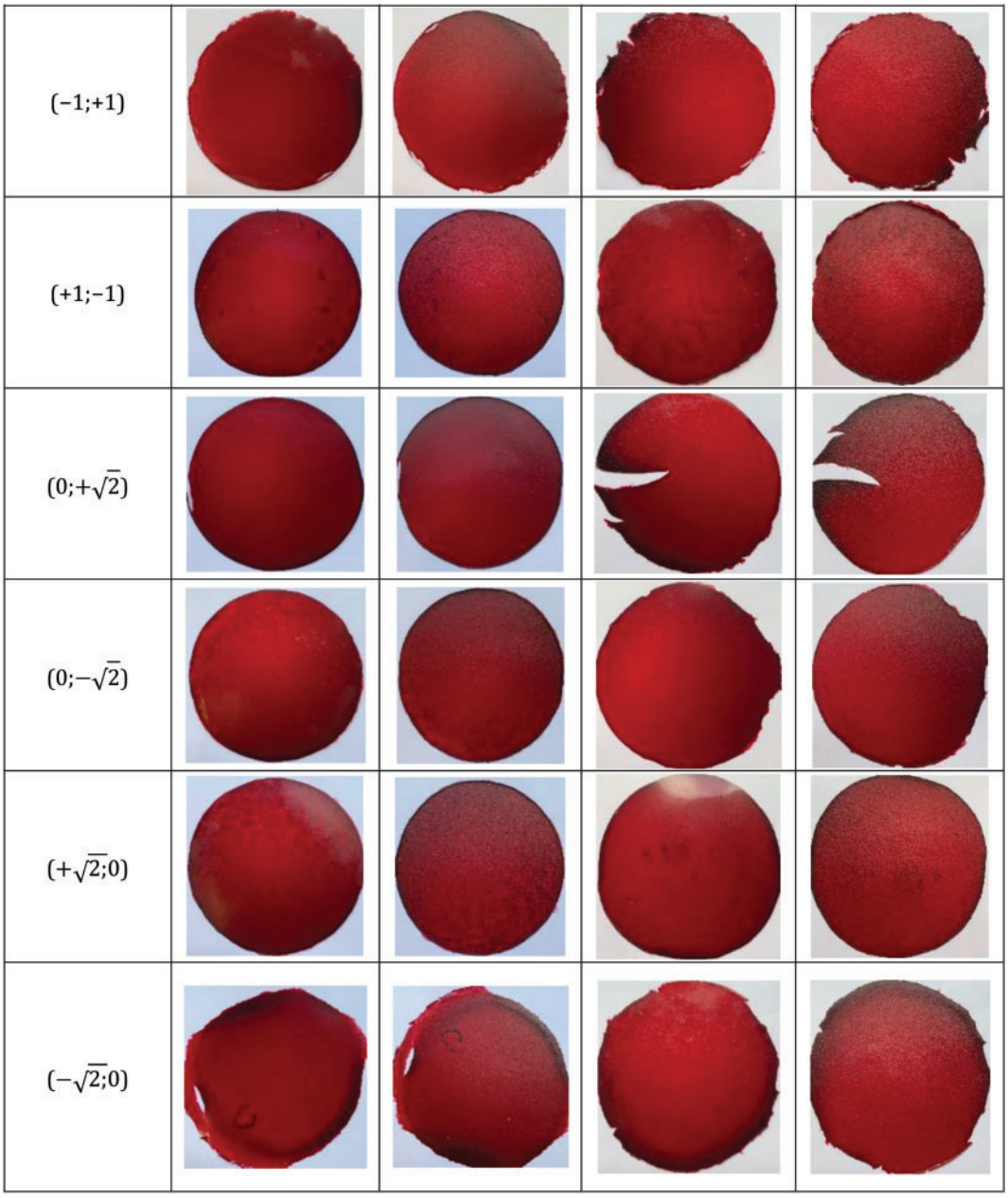

Figure 1: Photographs of films with various combinations of polysaccharides (carrageenan, starch and NC)

2.4 Film Characterization

2.4.1 Fourier-Transform Infrared Spectroscopy (FTIR)

The FTIR spectroscopy method was used to study the purity and structure of the obtained components and films, using an IRAffinity–1S spectrometer (Shimadzu, St. Petersburg, Russia) with an attenuated total reflection accessory, Quest Single Reflection ATR (Shimadzu, St. Petersburg, Russia), at ambient temperature. The resolution was 2 cm^{-1}, and the range was 500–4000 cm^{-1}.

2.4.2 Scanning Electron Microscopy (SEM)

The cross-sectional morphology of the films was studied using scanning electron microscopy (SEM) with a TESCAN VEGA microscope, model VEGA 3 LMU. The film samples were fractured after immersion in liquid nitrogen and then metallized with gold.

2.4.3 Thickness Measurements

The film thickness was measured using an electronic outside micrometer from Schut Geometrical Metrology Company. Measurements were taken at a minimum of eleven sample locations.

2.4.4 Contact Angle Measurements

The "sessile drop" method was used to measure the water contact angle using the Goniometer LK-1 instrument from NPK Open Science Ltd. (Krasnogorsk, Russia). The collected data were analyzed with the "DropShape" program, and the average values were presented. The experimental conditions were as follows: measurements were taken every 3–4 s after the deposition of a 2 μL water drop, and more than nine locations on the film surface were measured.

2.4.5 Mechanical Properties

The storage modulus values of films composed of unmodified polymers, with all other additives but without the addition of NC as reinforcement, were evaluated through dynamic mechanical analysis (DMA) using a TA Instruments DMA Q800 apparatus operating in tensile mode. The specimen was a thin rectangular strip with dimensions of approximately 40 mm × 5 mm × 1 mm. The tests were conducted under isochronous conditions at 1 Hz, with the temperature varying between 25°C and 50°C in 2°C increments. The films were conditioned in an atmosphere of 56% relative humidity in a desiccator containing a saturated calcium nitrate solution at 20°C.

To assess variations in mechanical properties due to differences in the carrageenan/starch mixture and nanocellulose content, a comparative mechanical test was conducted exclusively between the studied samples, without using any standard. The experimental conditions were defined to ensure all samples were tested under the same conditions.

2.4.6 Thermogravimetric Analysis (TGA)

The components used in the film formulations were analyzed by TGA in an air atmosphere only.

Films were examined using a DTG-60H apparatus (Shimadzu, Japan) under an air atmosphere with a flow rate of 30 mL/min, a heating rate of 10°C/min, a temperature range of 25°C–600°C, a sample mass between 5 and 7 mg, and aluminum pans.

The thermochemical properties of the films were determined under an Ar atmosphere with a flow rate of 50 mL/min using a TG 209 F1 Libra apparatus (Netzsch, Germany), with a heating rate of 10°C/min in the temperature range of 25°C–600°C, a sample mass between 1 and 3 mg, and aluminum pans.

2.4.7 Differential Scanning Calorimetry (DSC)

DSC analyses of the films were performed on a TA Instruments Q-20 using 6 mg of sample in aluminum pans. A first heating ramp was conducted from 25 to 160°C, followed by a second heating ramp from −70°C to 350°C under a nitrogen flow of 50 mL/min at a heating rate of 10°C/min.

2.4.8 Water Vapor Permeability (WVP)

The water vapor permeability of the films (WVP, g/(s·m·Pa)) was measured gravimetrically using a modified ASTM E96-95 method [38]. The film was sealed in a cell containing silica gel to achieve 0% relative humidity (RH) under the film. This cell was placed in a desiccator containing a saturated sodium chloride solution to maintain a relative humidity of 75%. The water vapor passing through the film and absorbed by the desiccant was determined by measuring the mass increase using Eq. (1).

$$WVP = (\Delta m * l)/(t * A * P * \Delta RH), \tag{1}$$

where Δm is the weight difference (g), l is the average film thickness (m); t is the experimental time (s), A is the area of penetration (the area of the bottle neck, m^2), P is the water vapor partial pressure at 25°C (3.169 kPa), and ΔRH is the relative humidity difference (0.75).

2.4.9 Oil Permeability (OP)

The oil permeability of the film was determined by placing an 8 cm × 2 cm film on a dried filter paper with a constant weight (w_i). Then, 25 drops of oil (m_{oil}) were applied to the film surface for 24 h without exceeding its edges. The film was then removed, and the filter paper was weighed (w_f). The oil permeability of the film was calculated using Eq. (2).

$$OP = (w_f - w_i)/m_{oil} * 100\% \tag{2}$$

2.4.10 Moisture Absorption (MA)

Moisture absorption (MA) of the films was determined by the Angles and Dufresne method [39]. Films (2 cm × 2 cm), dried to constant weight (w_i) at 60°C, were placed in a desiccator containing a saturated NaCl solution to maintain a relative humidity of 75%. The samples were weighed after 24 h (w_f), and MA was calculated using Eq. (3).

$$MA = (w_f - w_i)/w_f * 100\% \tag{3}$$

2.4.11 Water Solubility (Sw)

Water solubility (Sw) of the films was measured following the Bierhalz et al. method. Samples (2 cm × 2 cm), dried at 60°C for 24 h to constant weight (w_i), were immersed in vials containing 15 mL of distilled water for 1 h at 25°C. The films were then dried under the same conditions at 60°C for 24 h and weighed (w_f). Sw was calculated using Eq. (4).

$$Sw = (w_i - w_f)/w_i * 100\% \tag{4}$$

2.4.12 Film Light Transmission

Light transmittance (T), optical density (D), and film transparency were determined spectrophotometrically using a PE–5400UV spectrophotometer [38]. The light barrier properties of a 10 mm × 45 mm film sample were measured using a glass cuvette with air as a control at wavelengths between 350 and 750 nm. Light transmittance was calculated using Eq. (5).

$$T = 10^{-D} * 100\% \tag{5}$$

2.4.13 Film Color Depending on pH

To demonstrate the function of hibiscus flower extract as a pH indicator, films with optimal properties (compositions (−1; +1) and ($-\sqrt{2}$; 0)) were immersed in buffer solutions of different pH levels: potassium tetraoxalate ($KH_3C_4O_8{\cdot}2H_2O$) 0.05M (pH = 1.68), saturated potassium tartrate acid ($KC_4H_5O_6$) (pH = 3.56), potassium phthalate acid ($KC_8H_5O_4$) (pH = 4.01), potassium phosphate (KH_2PO_4) and sodium phosphate (Na_2HPO_4) (pH = 6.86), sodium tetraborate ($Na_2B_4O_7{\cdot}10H_2O$) (pH = 9.18), and saturated calcium oxyhydrate ($Ca(OH)_2$) (pH = 12.45). The color of the films and solutions was assessed every 10 min for up to 1 h.

2.4.14 Film Biodegradation

The biodegradability test was conducted on films with a carrageenan/starch matrix prepared without hibiscus extract and on films corresponding to the coordinates (0; 0) in the factorial space (Table 1), specifically those containing NC fibers (10 wt.%) or crystals (7 wt.%) together with hibiscus extract. The test was performed under controlled composting conditions in a laboratory environment following the ISO 20,200 standard [40,41]. The films (initial weight w_i) were placed in perforated material to ensure contact with microorganisms and moisture, facilitating easy removal after testing. They were then buried in a mixture containing 45% solid synthetic wet waste (10% compost, 30% rabbit feed, 10% starch, 5% sugar, 4% oil, 1% urea, 40% sawdust) and 55% water in a plastic container.

The samples underwent aerobic degradation at a controlled temperature of 28°C. Periodically, they were removed, dried under vacuum at 40°C for 2 h, and reweighed (w_f). A separate sample was taken for each measurement period, with at least three samples buried for each time point. The average results were presented. The degree of degradation (WL) was calculated by normalizing the sample mass on different composting days relative to the initial mass using Eq. (6).

$$WL = (w_i - w_f)/w_i * 100\% \tag{6}$$

Samples before and after extraction from the reactor were also analyzed by NMR. Structural analysis was performed using a Bruker Avance III 400 WB spectrometer (Bruker, Germany) at a magnetic field strength of 9.4 T with a 4 mm CP/MAS probe. A 100.64 MHz Larmor frequency was used to study ^{13}C nuclei.

2.4.15 Factorial Analysis

The results obtained in this set of experiments were analyzed using the Statgraphics (Statistical Graphics System) 7.0 software package. The software provided the ANOVA table, estimated effects, and predicted values for the studied variables. The effects of the variables and their interactions were analyzed concerning responses such as thickness, water contact angle, WVP, OP, MA, Sw, and storage modulus. Analysis of variance (ANOVA) was performed to eliminate non-significant effects. To ensure test reproducibility and validate the statistical results, experiments at the central point (level 0, 0) were repeated twice.

2.4.16 Statistical Analysis

Results were presented as mean ± standard deviation (SD) based on at least three parallel measurements. The normal distribution of the random variables was confirmed, and outliers were excluded from the analysis. The final analysis included the measured result, its random error, the total non-excluded systematic error, and the general error of the obtained results.

3 Results and Discussion

3.1 Structure Investigation

The structure of the reagents (starch and carrageenan, NC in the form of fibers and crystals, hibiscus flower extract, *Aloe vera*) and films was studied by FTIR spectroscopy (Fig. 2). Films with compositions corresponding to the coordinates (0; 0) of the factorial design (Table 1), namely, matrices of carrageenan/starch (50/50 wt.%), NC fibers (10 wt.%), or NC crystals (7 wt.%), were analyzed. This composition was chosen because it consists of equal amounts of polymers by mass and the average concentration of NC across the entire range.

The FTIR spectra of NC in the form of crystals and fibers correspond to the previously published FTIR spectrum of NC [42]. Broad peaks around 3340 cm^{-1} indicate the stretching frequency of O-H bonds from both free and intermolecular hydroxyl groups, which are involved in hydrogen bonding in cellulose. Peaks at 2897 cm^{-1} correspond to the stretching frequencies of C-H bonds, 1648 cm^{-1} is related to the vibrations of O-H bonds of absorbed water, 1429 cm^{-1} is related to the in-plane (scissoring) vibrations of C-H bonds in the methylene group of cellulose. Peaks around 1317 cm^{-1} show the bending vibrations of O-H bonds in the alcohol group, and the stretching frequency of C-O bonds in C-O-C pyranose is found at 1050 cm^{-1}. Peaks around 896 cm^{-1} are associated with β-glycosidic linkages [42,43].

The FTIR spectrum of hibiscus flower extract is also consistent with the previously published FTIR spectrum of hibiscus extract [44]. Spectral analysis reveals that the major functional groups of hibiscus include polysaccharides, suberin, and lipids [44]. The broad peak at 3400 cm^{-1} indicates the stretching frequency of O-H bonds from both free and intermolecular hydroxyl, which are involved in hydrogen bonding in polysaccharides. The peak at 1741 cm^{-1} corresponds to the stretching of the C=O bond in the ether group of lipids [44]. The peak at 1620 cm^{-1} is related to the stretching of the C=O bond in the amide group [45]. The peak at 1175 cm^{-1} shows asymmetric stretching vibrations of the C-O-C bond in suberin [44]. The peak at 1066 cm^{-1} corresponds to the stretching vibrations of the C-O bond in polysaccharides [44].

The FTIR spectrum of *Aloe vera* is also typical for this substance: 3305 cm^{-1} corresponds to the stretching vibrations of the O-H bond [46]; 2935 and 2881 cm^{-1} are asymmetric and symmetric stretching in the -CH_2 group, respectively [46,47]; 1714 cm^{-1} is C=O stretching from the carboxylic acid RCOOH [48]; 1625 cm^{-1} is asymmetric and symmetric stretching in the -COO- group of carboxylate compounds [48]; 1031 cm^{-1} can be assigned to -C-OH and -C-O bonds in polysaccharides [48]; <1000 cm^{-1} corresponds to aromatic -CH out-of-plane deformation [46,48].

The IR spectra of carrageenan and starch were found to be in agreement with those reported in the literature. For all samples, a broad peak in the range of 3600–3000 cm^{-1} corresponded to the valence OH vibration of the hydroxyl group of polysaccharides and water absorption [49]. Peaks in the range of 2950–2800 cm^{-1} are attributed to valence vibrations of C-H and are related to the lipophilicity of the material [50]. Peaks in the range of 700–1300 cm^{-1}, related to the carbohydrate region, are specific and allow the identification of each polysaccharide. The following characteristic peaks of starch were observed: 1637 cm^{-1} (C-O, associated with OH group or tightly bound water), 1421 cm^{-1} (symmetric deformation of CH_2), 1340 cm^{-1} (carboxyl groups), 1151 cm^{-1} (stretching of C-C and C-O), 1076 cm^{-1} (functional groups C-O), 996 cm^{-1} (stretching of C-O), and 927, 862, and 768 cm^{-1} (ring vibrations of C-O-C carbohydrate) [49,51]. Characteristic peaks for carrageenan were obtained: 1226 cm^{-1} (ether sulfate groups), 930 cm^{-1} (3,6-anhydrogalactose group), 845 cm^{-1} (galactose-4-sulfate), and 730 cm^{-1} (3,6-anhydro-D-galactose) [15].

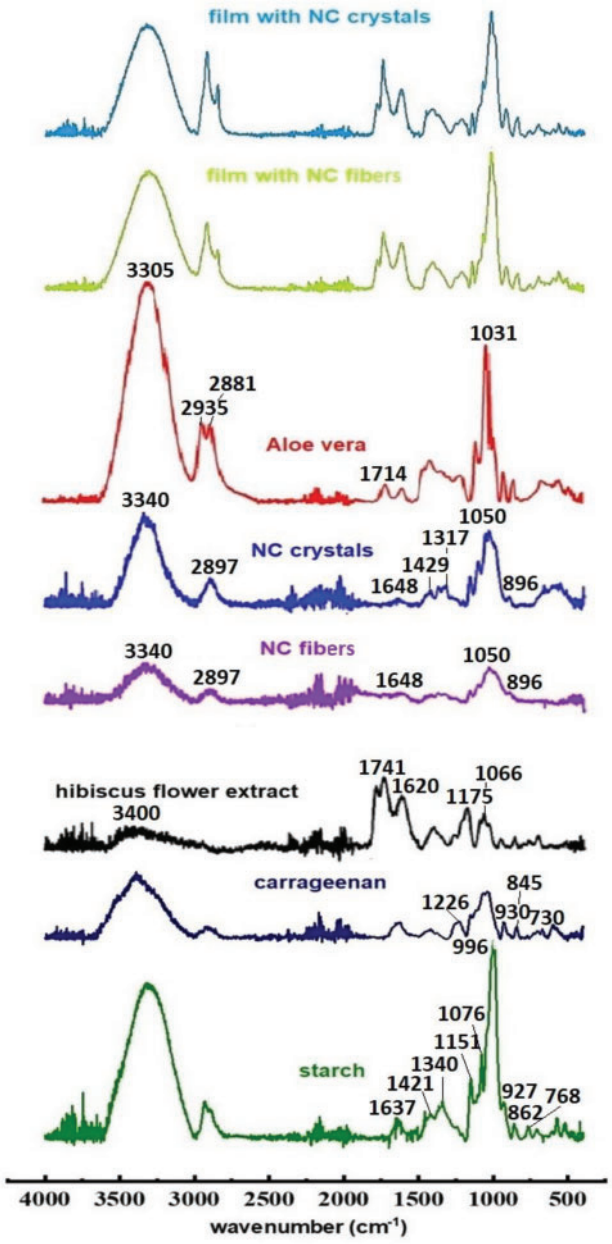

Figure 2: FTIR spectra of starch, carrageenan, NC, *Aloe vera*, hibiscus flower extract, and films with NC crystals and fibers

The FTIR spectra of the films with crystals and fibers are almost identical, and their peaks correspond to the peaks of the individual components. Peaks in the range of 3600–3000 cm^{-1} correspond to the valence vibration of the hydroxyl (-OH) group of polysaccharides (carrageenan, starch, and NC), *Aloe vera*, and hibiscus flower extract (Fig. 2). Peaks in the range of 2950–2800 cm^{-1} are related to valence vibrations of C-H. Peaks at 1151 cm^{-1} correspond to starch (stretching of C-C and C-O), peaks at 846 cm^{-1} correspond to carrageenan (galactose-4-sulfate), and peaks at 924 cm^{-1} are related to starch (ring vibrations of C-O-C carbohydrate). In addition, a new characteristic peak appears in the FTIR spectra of the films, which is not present in the FTIR spectra of the polysaccharides (carrageenan, starch, and NC). This peak at

1740 cm^{-1} corresponds to the stretching of the C=O bond of the ether group in lipids in hibiscus flower extract (Fig. 2) [44].

SEM cross-sectional micrographs of the films at different magnifications containing NC fibers and crystals are presented in Fig. 3.

SEM micrographs showed that most of the films had good homogeneity with a uniform distribution of NC particles in the polymer matrix (no obvious NC particles were present). To avoid aggregation, NC was used in the form of an aqueous dispersion and was not dried, which suppressed its agglomeration in the polymer matrix to some extent [52]. Holes were observed in some samples due to the presence of air bubbles trapped during film preparation. In general, the blends were compatible, resulting in visually homogeneous films without phase separation [53]. The cross-sectional structure of the films containing NC crystals differs from that of the films containing NC fibers and shows a "wavy" morphology, the intensity of which increases with increasing carrageenan or NC crystal content. In addition, as the concentration of NC fibers in the films increases, the size and number of "defects" or "indentations" in the cross-sectional structure also increase. Films containing NC crystals show significantly fewer "defects" or "indentations" in the cross-sectional structure. This behavior may be related to the amount and size of NC used as a reinforcing agent, with NC fibers having larger dimensions than NC crystals, in addition to the fact that the NC fiber content was higher.

3.2 Investigation of Physicochemical, Thermal and Mechanical Properties

The main parameters such as thickness, water vapor permeability (WVP), oil permeability (OP), water solubility (Sw), moisture absorption (MA), and water contact angle were studied, as they are necessary to evaluate the potential of using films as packaging materials. The effect of carrageenan content (X) and NC loading (Y) (both linear (X or Y) and quadratic (X^2 or Y^2)) on the observed responses (film parameters) was analyzed using response surface methodology (RSM). The data obtained for these parameters are presented in Table 3 and Table S1 of the Supplementary Materials (values obtained for thickness, WVP, and OP).

The values of water contact angle, Sw and MA are related as they reflect the polar/non-polar nature of the films. If films have low water contact angles, it indicates that they are more polar and therefore have a good affinity for water, making them easier to wet, absorb more moisture, and dissolve faster. With regard to the use of films for food packaging that may come into contact with water, it is preferable to obtain films that are less soluble, absorb less moisture and have a more non-polar character (i.e., higher contact angle). To assess the hydrophilic-hydrophobic balance of the film surfaces, the water contact angles of the films were measured (Fig. 4).

The statistical treatments revealed that for films with NC fibers, the only significant variable was the carrageenan content (based on ANOVA and the Pareto chart, it crossed the reference line with a p-value of 0.05). Therefore, the variation in this matrix component has a significant effect on the contact angle values. For films with NC fibers, the lowest water contact angle values were obtained at intermediate (average) concentrations of carrageenan [54] and NC fibers. For films containing NC crystals, no variable had a significant effect, as indicated by ANOVA and the Pareto chart, which did not cross the reference line at a p-value of 0.05. This suggests that changes in composition do not significantly affect the contact angle values. The lowest water contact angle values for films with NC crystals were obtained at central (average) concentrations of carrageenan, regardless of the NC crystal content. In these lowest ranges, the films are more polar. However, the contact angles for all films are less than 90°, indicating that water wets the film and has a good affinity for it due to their similar chemical nature. Comparing the water contact angle values of films with NC crystals and fibers, it was shown that films with NC crystals were more polar (with lower contact angle values). The moisture absorption (MA) parameter of the films was also statistically evaluated (Fig. 5).

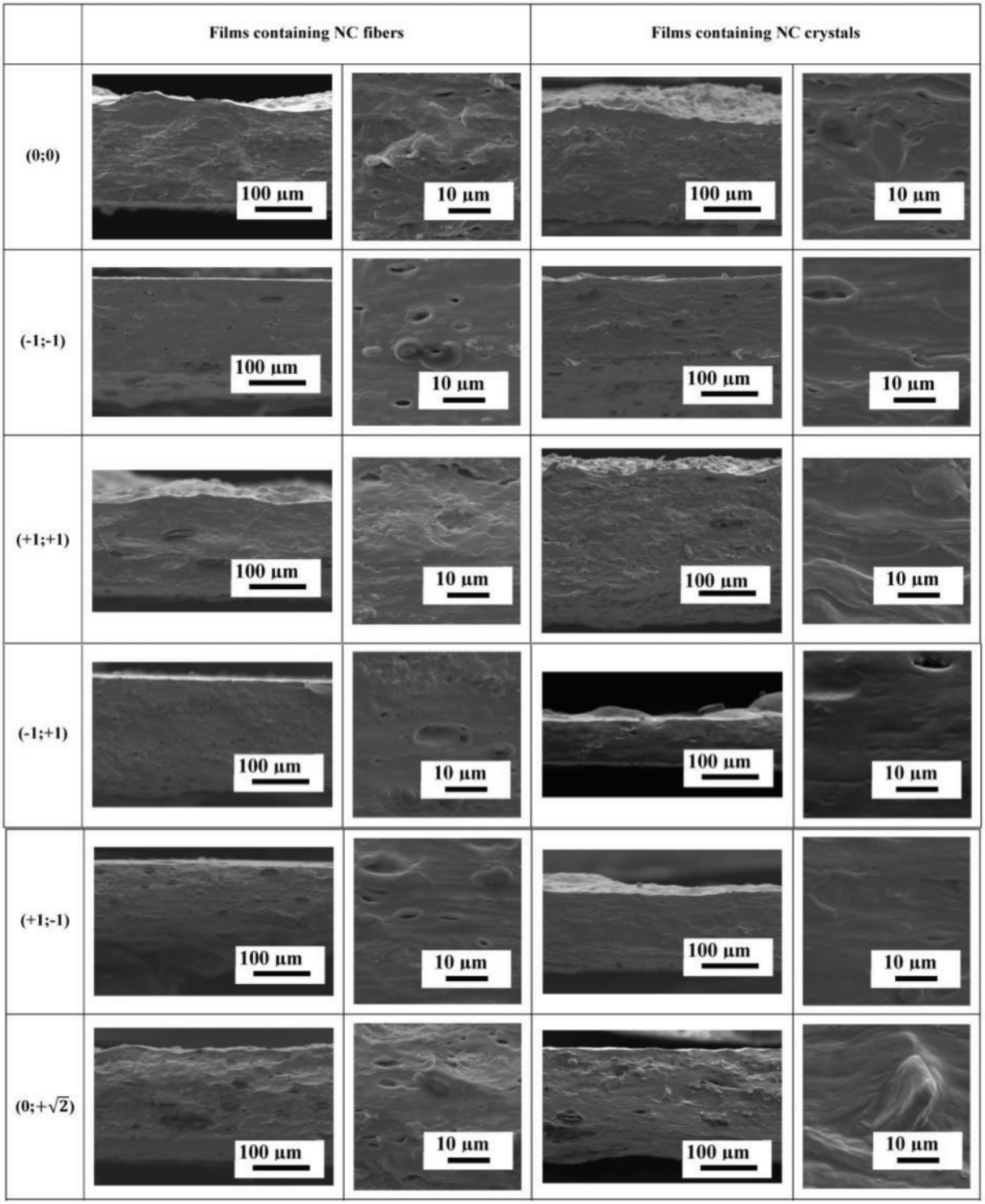

Figure 3: (Continued)

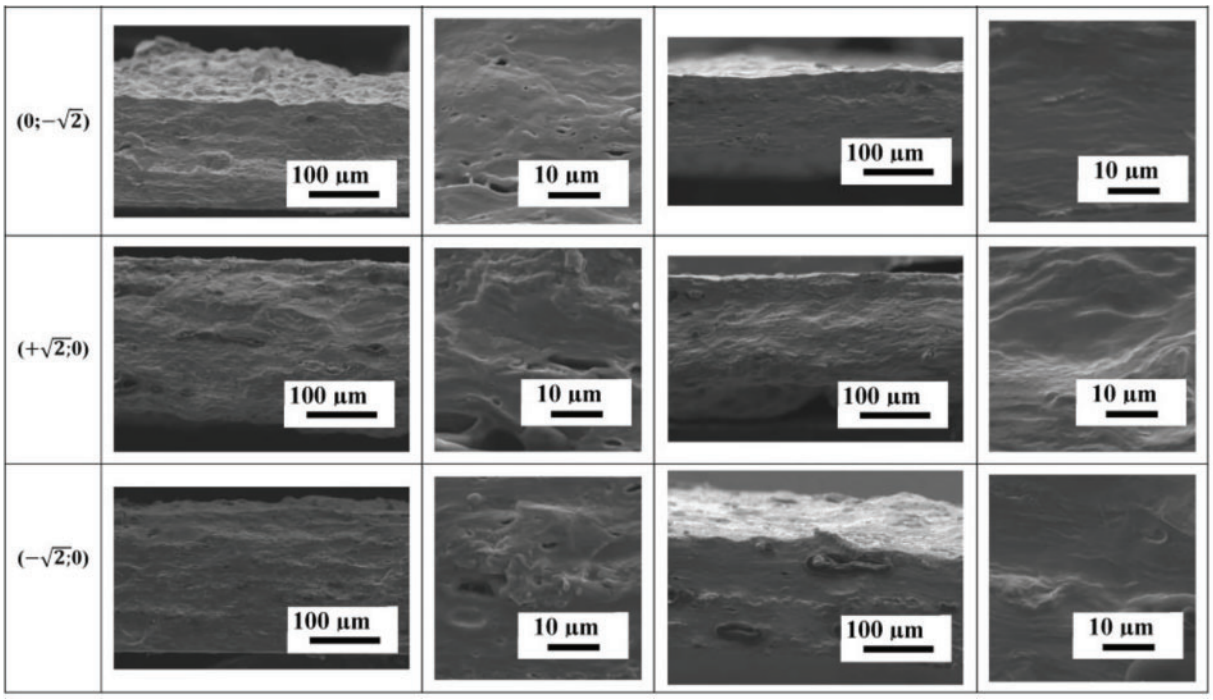

Figure 3: SEM cross-sectional micrographs of films containing NC fibers and crystals

Table 3: Values of water solubility (Sw), Moisture Absorption (MA), and contact angle of water for the films prepared with NC fibers and crystals

	Sample	Sw (%)	MA (%)	Contact angle (°)
NC fibers	**(0; 0)**	56 ± 5	19 ± 1	51 ± 2
	(−1; −1)	53 ± 5	17 ± 1	64 ± 2
	(+1; +1)	66 ± 5	21 ± 1	74 ± 2
	(−1; +1)	54 ± 5	18 ± 1	67 ± 3
	(+1; −1)	66 ± 5	19 ± 1	66 ± 1
	(0; +√2)	58 ± 5	18 ± 1	59 ± 1
	(0; −√2)	61 ± 5	19 ± 1	51 ± 2
	(+√2; 0)	65 ± 5	21 ± 1	56 ± 3
	(−√2; 0)	55 ± 5	16 ± 1	73 ± 1
NC crystals	**(0; 0)**	59 ± 5	18 ± 1	40 ± 2
	(−1; −1)	49 ± 5	16 ± 1	58 ± 2
	(+1; +1)	60 ± 5	21 ± 1	38 ± 1
	(−1; +1)	54 ± 5	16 ± 1	58 ± 1
	(+1; −1)	65 ± 5	21 ± 1	39 ± 3
	(0; +√2)	61 ± 5	18 ± 1	25 ± 1
	(0; −√2)	63 ± 5	18 ± 1	20 ± 4
	(+√2; 0)	66 ± 5	20 ± 1	51 ± 1
	(−√2; 0)	56 ± 5	14 ± 1	55 ± 1

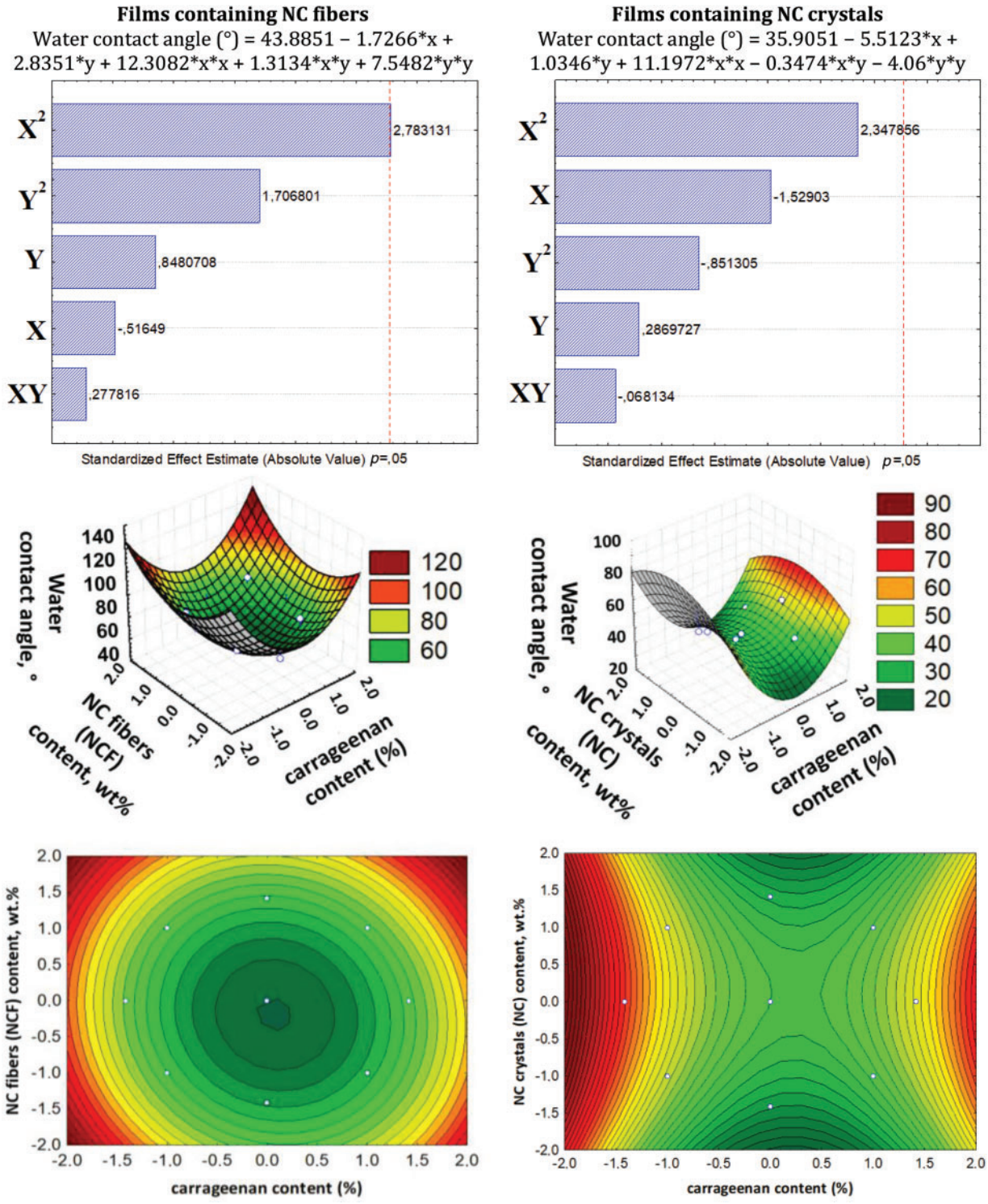

Figure 4: Pareto charts, 3D surface plots, and contour plots showing the dependence of the water contact angle of films on NC and carrageenan content

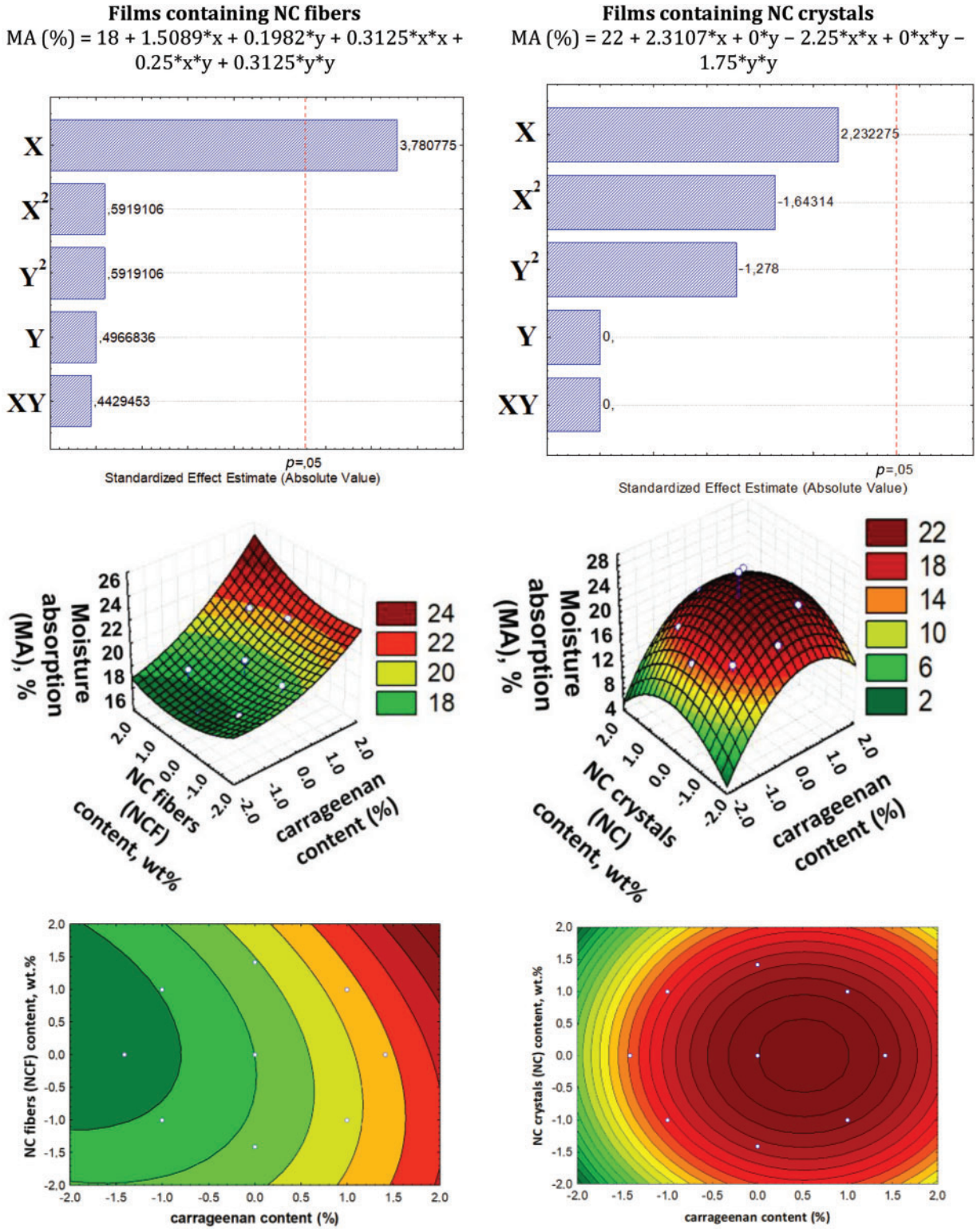

Figure 5: Pareto chart, 3D surface plot, and contour plot showing the dependence of moisture absorption in films on NC and carrageenan content

The statistical treatments showed that the carrageenan content variable is significant and has a positive effect on the MA parameter for films containing NC fibers (confirmed by ANOVA and Pareto chart): the increase in carrageenan leads to a higher MA. This behavior is due to the fact that carrageenan has higher solubility in water than starch and, therefore, absorbs moisture more easily [54]. For films containing NC crystals, none of the variables showed any significant effects. The statistical treatment data for film solubility in water (Sw) are presented in Fig. 6.

The statistical treatments showed that for films with both NC fibers and crystals, the carrageenan content variable is significant and has a positive effect on solubility. This means that increasing the carrageenan content leads to higher solubility of the films, due to the high solubility of carrageenan in water compared to starch [55].

Based on the results of the statistical analysis (ANOVA and Pareto chart) for the thickness of the films (Table S1 of Supplementary Materials), it was verified that the variables (carrageenan and NC contents) did not have a significant effect on the thickness response [56] (p-value higher than 0.05, as shown in Fig. S1 of Supplementary Materials).

When packaging or coating fruits/vegetables, it is important that the films block the passage of water vapor as much as possible to prevent moisture loss in the food products. The gravimetric method was used to measure the water vapor permeability of the films (WVP) (Table S1 of Supplementary Materials). The result of the statistical treatment is presented in Fig. S2 of Supplementary Materials. The statistical treatments showed that no variable had a significant effect on films with NC crystals (confirmed by ANOVA and Pareto chart), indicating that changes in composition did not significantly affect the WVP values. However, the carrageenan content variable was found to have a significant impact on the WVP values of films containing NC fibers. In the Pareto chart (Fig. S2 of the Supplementary Materials), the effect of carrageenan content is 5.47319 for films with NC fibers, indicating that it significantly influences the response; specifically, increasing the carrageenan content leads to an increase in WVP [55]. The region with the highest WVP is the region with the highest carrageenan content. Comparing the values for the two film types (Table S1 of the Supplementary Materials), films containing crystals exhibited lower WVP values. This can be explained by two factors. First, NC fibers were used in higher concentrations in the formulations compared to NC crystals, and the presence of higher filler content could render the structure more susceptible to water permeation. The other effect may be related to the size of the NC particles. NC crystals are much smaller and dispersed individually, whereas the NC fibers, due to their structure, can form a network with channels for transport. Thus, in films with NC crystals, water molecules find it more difficult to follow the path within the film, but with fibers, this path can be facilitated. NC crystals are known to be a reinforcing filler, which also leads to an improvement in the barrier properties of the composite against air, oxygen, and water vapor [57–59].

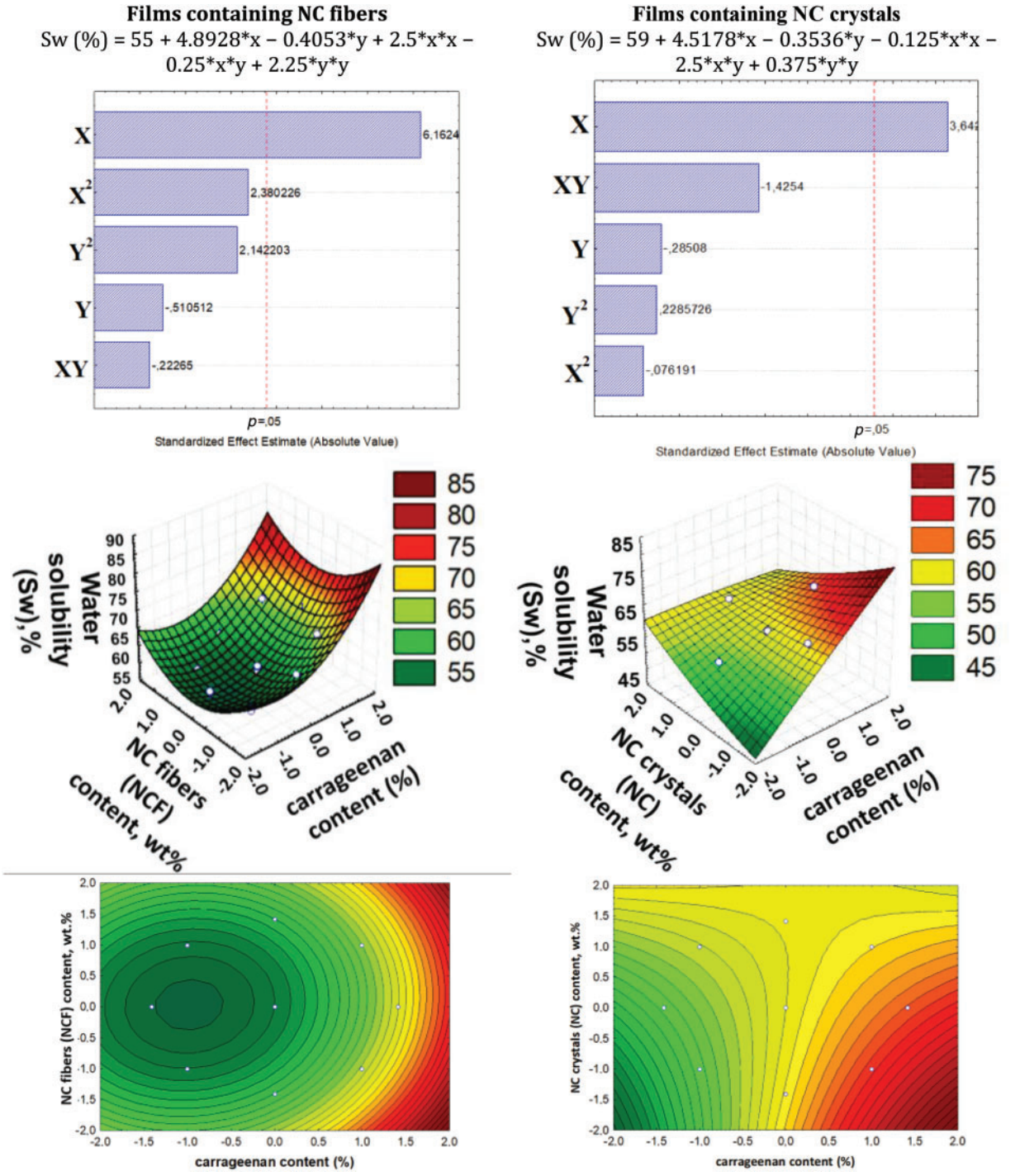

Figure 6: Pareto charts, 3D surface plots, and contour plots showing the dependence of the solubility in water of films on NC and carrageenan content

Oil permeability tests also show the chemical nature of the films, as more polar films do not allow oil to pass through but repel it (Table S1 of Supplementary Materials). This property must behave oppositely to that observed for WVP, as it changes the polar character of water to the non-polar character of oil. The

result of the statistical treatment for oil permeability is shown in Fig. S3 of Supplementary Materials. It was verified that films with NC crystals showed the same result regardless of the compositions, and this was demonstrated by the statistical treatments in which the variables did not show significant effects on the oil permeability response. However, for films with NC fibers, the two significant variables were the carrageenan content (quadratic X^2) and the NC fiber content (quadratic Y^2). The values obtained in the Pareto chart are negative (−9.14446 and −8.55687, respectively), showing that increasing these values reduces oil permeability (Fig. S3 of Supplementary Materials). This is consistent with and contrary to what is observed for WVP. This may also be related to the fact that films with NC crystals have a higher polarity (smaller water contact angle) than films with NC fibers (Fig. 4) and repel non-polar compounds (oil) more strongly.

Good mechanical properties are also necessary for high-quality packaging. The results obtained for the storage modulus of the films at 35°C are presented in Table 4, and the statistical treatments for this property are presented in Fig. 7.

Table 4: Values obtained for storage modulus from DMA, as well as the glass transition temperature of thermoplastic starch and the melting temperature of myristic acid, obtained from DSC for the films prepared with NC fibers and crystals

	Sample	Storage Modulus (MPa)	Tg starch (°C)	Myristic acid melting temperture (°C)
NC fibers	**(0; 0)**	93.17	−26	48.5
	(−1; −1)	26.62	−25	47.9
	(+1; +1)	102.98	−26	49.8
	(−1; +1)	104.35	−25	49.1
	(+1; −1)	119.78	−26	48.5
	(0; $+\sqrt{2}$)	75.00	−23	50.1
	(0; $-\sqrt{2}$)	41.25	−25	49.5
	($+\sqrt{2}$; 0)	110.30	−21	49.6
	($-\sqrt{2}$; 0)	37.51	−26	48.2
NC crystals	**(0; 0)**	74.92	−28	50.3
	(−1; −1)	30.45	−26	49.2
	(+1; +1)	16.69	−27	48.9
	(−1; +1)	58.11	−21	55.0
	(+1; −1)	59.98	−21	48.6
	(0; $+\sqrt{2}$)	40.45	−16	49.9
	(0; $-\sqrt{2}$)	48.54	−23	48.3
	($+\sqrt{2}$; 0)	52.70	−27	48.4
	($-\sqrt{2}$; 0)	22.77	−27	48.1

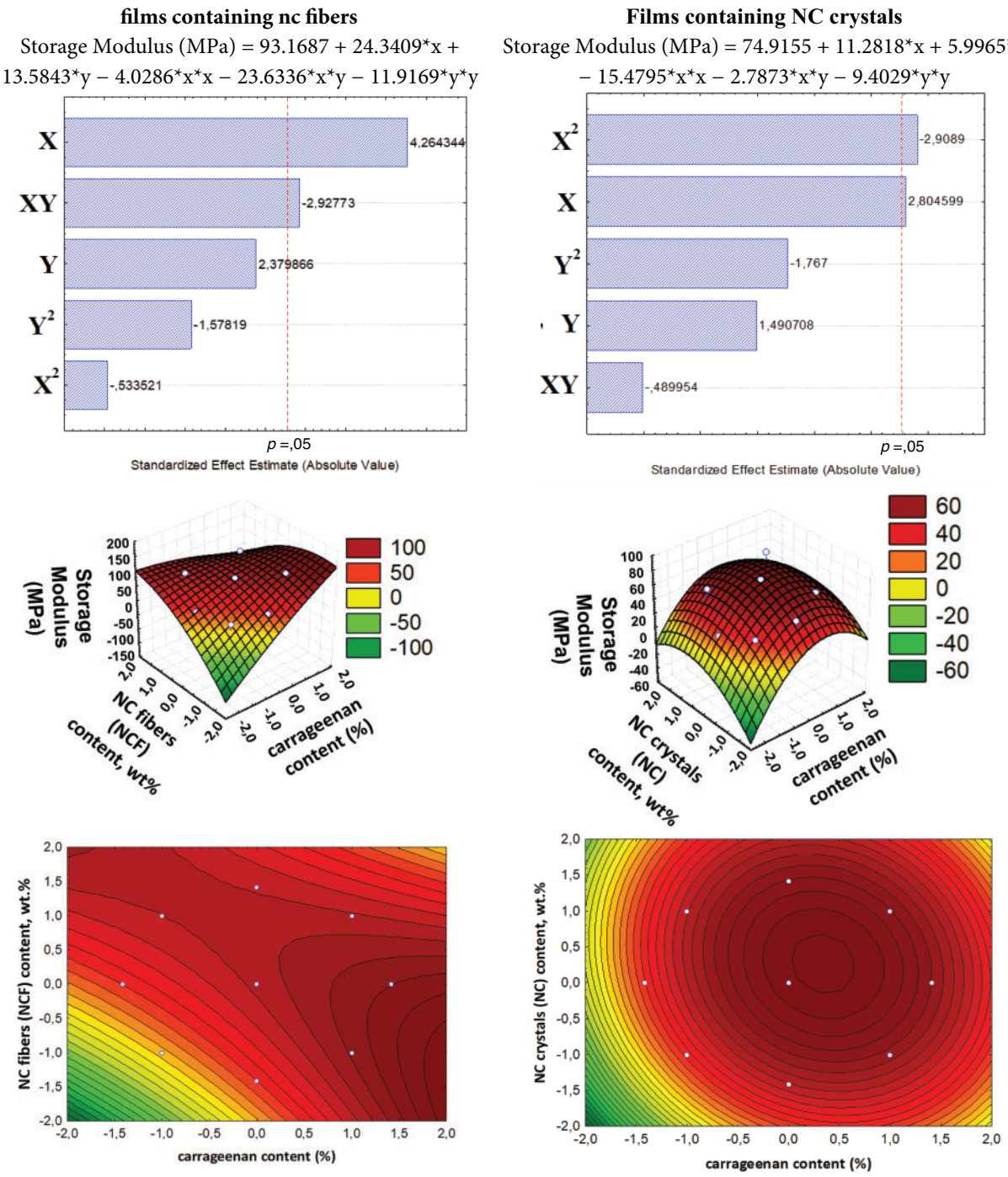

Figure 7: Dependence of storage modulus for films with NC fibers and crystals on carrageenan and NC content

From the statistical treatments, it was verified that for films with NC crystals, the carrageenan content variable, both linear and quadratic (X and X^2), had a significant effect on the storage modulus values. The linear variable has a positive effect (+2.804599), indicating that greater carrageenan content results in increased storage modulus. However, the quadratic variable has a negative effect (−2.9089), leading to a reduction in the storage modulus. Therefore, considering that the effect of the quadratic variable is

numerically greater than the linear one, it will result in a reduction in storage modulus values for both higher and lower levels of carrageenan. This can be seen in the response surface plot, where the extreme regions of the surface show a decrease in storage modulus values.

For films with NC fibers, the linear carrageenan content (X) and the ratio between the linear carrageenan content and the linear NC fiber content (XY) have a significant effect on the storage modulus values. The linear variable of carrageenan content has a positive effect (+4.264344), indicating that an increase in carrageenan content leads to a corresponding increase in storage modulus. However, the XY ratio negatively affects (−2.92773), leading to a reduction in storage modulus. Numerically, the effect of the linear variable of carrageenan content is greater than that of the XY ratio; higher carrageenan content results in an increase in storage modulus values. However, combinations of lower carrageenan and NC fiber contents (−1; −1) or higher carrageenan and NC fiber contents (+1; +1) may contribute to a reduction in storage modulus values. This can be seen in the response surface plot, where the regions with combinations of points (−1; −1) and (+1; +1) show a decrease in storage modulus values.

Overall, the films with NC crystals had lower storage modulus values than the films with NC fibers. This may be due to the higher content of NC fibers used in the film formulations. Additionally, the storage modulus values of film formulations made with pure polymers—without the addition of NC as reinforcement but including all other additives—were also evaluated. As a result, the values obtained for the film made from starch and carrageenan were 44.90 and 40.46 MPa, respectively. The films made from the polymer blend (carrageenan/starch) and with the addition of NC generally had increased storage modulus values compared to films made from pure polymers. This increase was mainly due to the addition of NC as a reinforcing agent. However, it was noted that in some regions, even with the addition of higher levels of NC, low storage modulus values were observed, as in regions with low levels of carrageenan. This reduction, even with a reasonable level of NC, may have been caused by the immiscibility of the carrageenan and starch mixture in formulations with lower levels of carrageenan or by the formation of structures with holes from air bubbles, as confirmed by the SEM data (Fig. 3). Therefore, the presence of these structures may have a negative effect on the storage modulus values.

To study the miscibility of the polymers used in the formulations, DSC tests were carried out. The data obtained are presented in Fig. S4 of the Supplementary Materials. It was shown that a small endothermic peak between 40°C and 60°C was attributed to the melting of myristic acid (melting temperature of 54.4°C). The melting temperature values of the peak, ranging from 48.1°C to 55.0°C for each film, are presented in Table 4. During the second heating scan, the presence of a thermal event related to the glass transition of the thermoplastic starch was observed in the range of −10°C to −30°C. The values obtained for each sample are shown in Table 4. From the Tg values of the starch, the temperature variations were very small, indicating that there was probably no miscibility of starch and carrageenan in the blend formed. The term "miscibility" refers to the extent to which the polymers in a blend are dispersed in one another and the interactions between them, which are highly temperature-dependent [60]. The SEM data also confirm that the two polymers exhibit good compatibility. The term "compatibility" refers to the final properties of the polymer blend with enhanced properties. To avoid the effect of the presence of immiscibility between starch and carrageenan, a physical approach was used by incorporating compatible agents (e.g., nanocellulose, etc.). In conclusion, starch and carrageenan are compatible but not miscible.

The thermochemical properties of the films and their pristine components were determined by TGA under an Ar and air atmosphere (Fig. S5 of Supplementary Materials). The TGA curves of the film show similar profiles, with stages of degradation related to their main pristine components (starch, carrageenan, and hibiscus extract, which is around 1 g in the formulations and would represent 50% of the mass of the polymers). The components with significant content are glycerol and NC. The minor variations in film

degradation temperatures at each stage can be primarily attributed to differences in composition, particularly the content of starch and carrageenan, and to a lesser extent, NC.

From the data obtained, it can be concluded that the most suitable formulations for packaging are those with lower carrageenan content and higher NC content. These are the composition conditions $(-\sqrt{2}; 0)$ and $(-1; +1)$, as these formulations have shown properties of greater water resistance, higher hydrophobicity, lower water vapor permeability, and better mechanical properties. These properties are essential for food packaging, which must be both mechanically resistant and resistant to the presence of water.

3.3 Optical Properties of Films

The optical density, light transmission, and transparency of the films were measured at wavelengths ranging from 350 to 750 nm. The choice of this wavelength range was made to study the films' behavior under visible and UV radiation. For visible light, the short-wavelength limit is considered to be between 380–400 nm, while the long-wavelength limit is 760–780 nm (although visible radiation can extend up to 810 nm). The UV spectrum covers wavelengths from 100 to 400 nm, divided into three distinct regions: UV-A (315–400 nm), UV-B (280–315 nm), and UV-C (100–280 nm). As sunlight passes through the atmosphere, all UV-C radiation and 90% of UV-B radiation are absorbed by carbon dioxide, water vapor, ozone, and oxygen. Therefore, the UV radiation that reaches the Earth's surface consists mainly of UV-A rays and a small amount of UV-B rays.

From the statistical treatments and ANOVA (not shown here), it was verified that no variable had a significant effect on the optical density of any film (whether containing NC fiber or NC crystal) at any evaluated wavelength. Thus, variations in the composition of the carrageenan/starch mixture and in NC content do not appear to affect the optical density, as evidenced by the thickness measurements. The optical density data obtained are shown in Fig. 8.

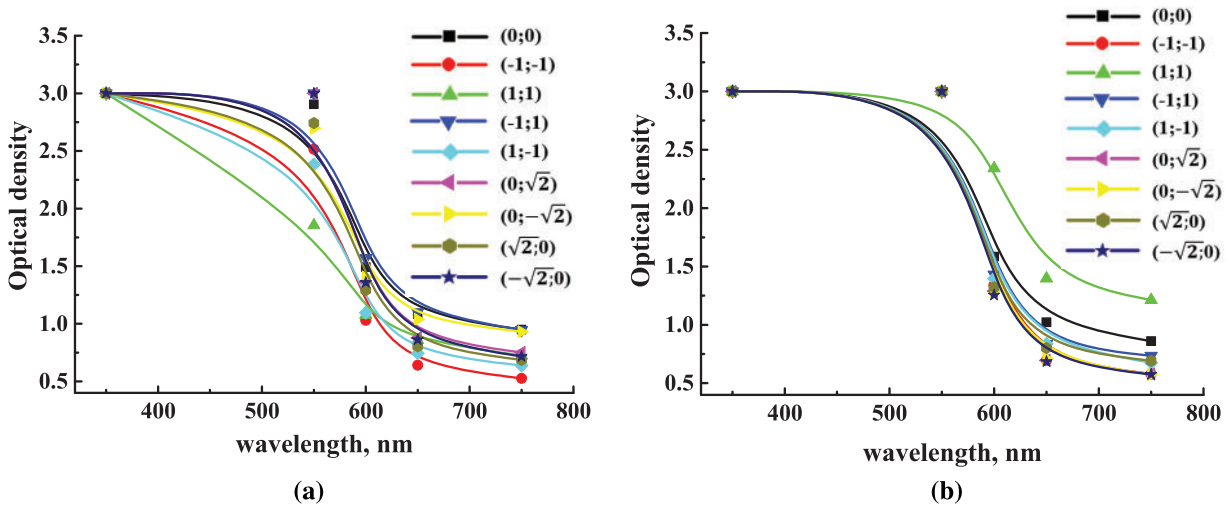

Figure 8: Optical density of films with (a) NC fibers and (b) NC crystals

The films containing NC fibers exhibited the highest optical densities at 350 nm, completely blocking radiation at this wavelength. This demonstrates that the films serve as excellent barriers to UV radiation. From 550 to 600 nm, these films showed reduced optical densities, allowing a small amount of radiation to pass through. Low optical densities were observed at 650 and 750 nm.

The films with NC crystals displayed high optical densities at both 350 and 550 nm, confirming complete blockage of radiation at these wavelengths. This indicates that films with NC crystal offer a higher barrier to UV radiation compared to films containing NC fibers. These results suggest that films containing NC crystal possess radiation-blocking properties at wavelengths corresponding to the colors violet, blue, cyan, and green (ranging from 400 to 565 nm), which may provide valuable characteristics for their potential applications. The optical density values began to decrease at 600 nm, with low values recorded at 650 and 750 nm. Light transmission values were calculated based on the optical densities obtained for the films (Fig. 8).

Considering that the films act as a barrier in the UV range, this opens new possibilities for their application. For example, they could be used directly on fruits and vegetables in plantations (i.e., pre-harvest) as a UV protective barrier, preventing significant losses due to sunburn, which can cause severe economic damage to producers.

The films exhibited low light transmission in the UV range (up to 400 nm) (Fig. 9). Therefore, when used as packaging material, these films can serve as a UV radiation barrier, helping to reduce oxidation reactions in packaged or coated food products. As the wavelength increases within the visible range (400–750 nm), the light transmission of the films also increases, reaching up to 30%. For food packaging applications, it is crucial that the films do not completely block light in this range, as transparency allows consumers to see the product inside. The developed films meet this requirement, as indicated by the light transmission values obtained at the tested wavelengths in the visible range.

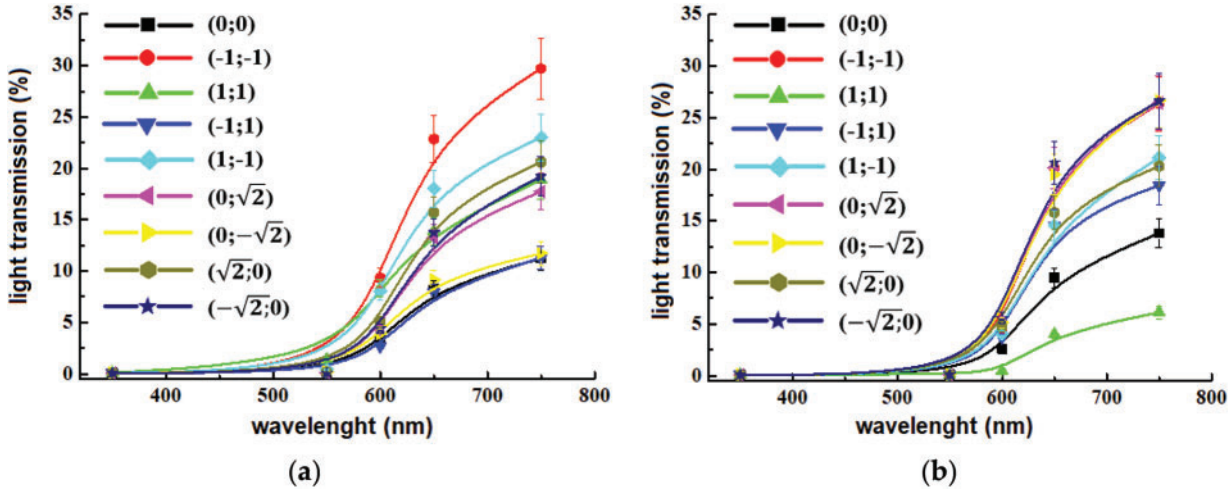

Figure 9: Light transmission properties of films containing (a) NC fibers and (b) NC crystals

3.4 Investigation of Activity of Incorporated Film Additive

To demonstrate the function of hibiscus flower extract as a pH indicator, films with optimal properties ($(-\sqrt{2}; 0)$ and $(-1; +1)$) were immersed in buffer solutions of different pH, and their color was assessed every 10 min. The color of the films and solutions changed after 10 min of exposure. Fig. 10 presents photographs of the solutions after 1 h, illustrating the color change as a function of pH.

The hibiscus flower extract incorporated into the films was shown to change color from pink to brown in solutions ranging from acidic to alkaline. This confirmed that the developed films responded to pH variations by changing color. However, further testing with different products is necessary to validate this effect.

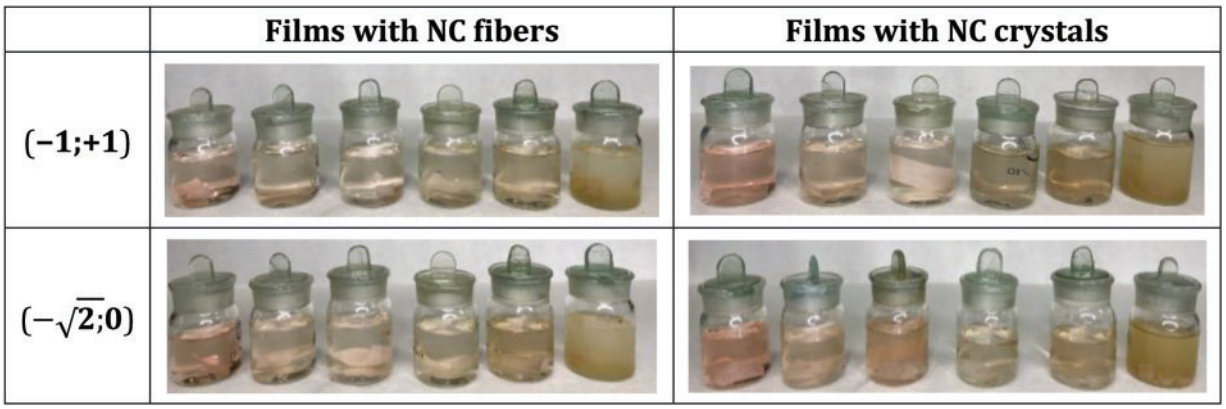

Figure 10: Photos of the resulting solutions after 1 h, showing the color change depending on pH (from left to right: solutions with pH 1.68, 3.56, 4.01, 6.86, 9.18, 12.45)

3.5 Investigation of Film Biodegradability

During the first week of the biodegradation experiment, the films showed slight deformation, turned yellow-brown, and became more opaque. These changes indicate water absorption and the formation of low molecular weight compounds due to the hydrolytic degradation process [61]. As the exposure time in the medium increased, the films continued to deform, collapse, and darken to a deep brown color. Meanwhile, the compost medium facilitated the formation of humus-rich soil (darkening) due to microbial activity [62]. The decomposition of the films was also assessed based on weight loss as a function of composting time (Fig. 11).

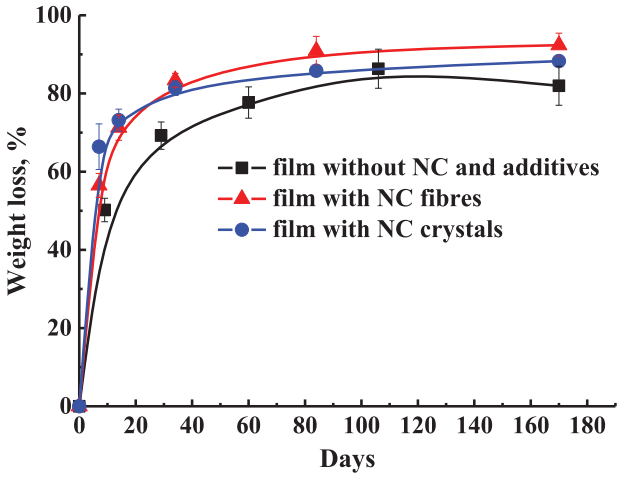

Figure 11: Film decomposition curves under composting conditions

The NMR spectra of the samples before and after extraction, along with the structure of the glucose unit of starch, are presented in Fig. 12.

The spectrum of the film before testing can be described as the sum of the spectra of its main components—carrageenan and starch. Additionally, two narrow intense lines at 64 and 73 ppm are observed in the spectrum. These peaks may correspond to the C5 and C6 carbon atoms of the glucose units in starch (Fig. 12b), which can be terminal and located in amorphous phases where water is retained. This water retention may allow for rapid vibrational and rotational motion. From the spectra of the films after extraction

from the reactor, it can be concluded that prolonged exposure in the medium leads to a gradual reduction in starch content until it disappears completely. The absence of the previously observed narrow peaks in these spectra indicates that the films become brittle, and the water-saturated amorphous phase disappears.

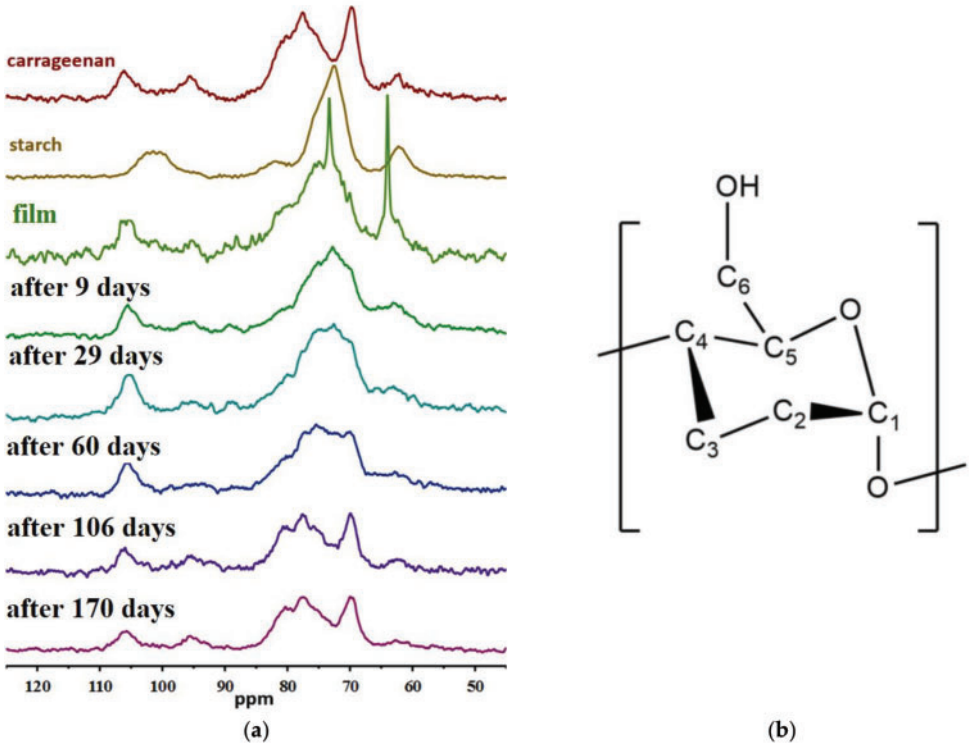

Figure 12: (a) ^{13}C NMR spectra of samples and (b) structure of the glucose unit of starch

4 Conclusions

In this study, an innovative food packaging film was developed using starch, carrageenan, nanocellulose (fibers or crystals), *Aloe vera*, and hibiscus flower extract. To determine the optimal concentrations of the film components for improved performance in food packaging, different compositions were evaluated, and a detailed analysis was conducted. Increasing the carrageenan content in the matrix significantly improved the films' wettability, moisture absorption, solubility, and water vapor permeability. Additionally, the incorporation of nanocellulose and carrageenan enhanced the mechanical properties. The starch/carrageenan films demonstrated effective UV radiation barrier properties and excellent biodegradability over a period of 170 days. The additives introduced (*Aloe vera* gel and hibiscus flower extract) provided the films with functional properties, namely antibacterial activity and the ability to change color according to the pH of the environment (experiments to be conducted as part of future research). Based on the data obtained, the most suitable formulations for packaging are those with lower carrageenan content and higher NC content, as they exhibit greater water resistance, hydrophobicity, lower water vapor permeability, and better mechanical properties. However, the films showed water solubility and moisture absorption values of over 53% and 14%, respectively. Therefore, they are not suitable for packaging foods with wet surfaces and high moisture content (e.g., seafood, meat) or for use in humid environments. Future research should focus on applying this optimized edible film composition in food packaging testing and applications.

Acknowledgement: The experimental work was facilitated by the equipment from the Resource Centers for Nanotechnology, Magnetic Resonance, Thermogravimetric and Calorimetric Research Centre, Centre for Innovative Technologies of Composite Nanomaterials, Chemical Analysis and Materials Research Centre, and Centre "Nanofabrication of Photoactive Materials (Nanophotonics)" at the St. Petersburg State University.

Funding Statement: This research was funded by the Russian Federation represented by the Ministry of Science and Higher Education, Russia, grant number 075-15-2022-1231 on 18.10.2022; National Research Foundation (NRF), South Africa, grant number 150508; Brazilian National Council for Scientific and Technological Development (CNPq), Brazil, grant number 440057/2022-1.

Author Contributions: The authors confirm contribution to the paper as follows: study conception and design: Mariia Dmitrenko, Daniel Pasquini, Sabu Thomas, Anastasia Penkova; methodology: Daniel Pasquini, Andrey Terentyev, Alexander Dyachkov, K. S. Joshy, Maya Jacob John, Sabu Thomas, Anastasia Penkova; data collection: Mariia Dmitrenko, Daniel Pasquini, Marcela Piassi Bernardo, João Marcelo de Lima Alves, Anna Kuzminova, Ilnur Dzhakashov, Andrey Terentyev, Alexander Dyachkov; analysis and interpretation of results: Mariia Dmitrenko, Daniel Pasquini, Anastasia Penkova; draft manuscript preparation: Mariia Dmitrenko, Daniel Pasquini; writing—review and editing: Mariia Dmitrenko, Daniel Pasquini, Marcela Piassi Bernardo, João Marcelo de Lima Alves, Anastasia Penkova. All authors reviewed the results and approved the final version of the manuscript.

Availability of Data and Materials: Data available on request from the authors.

Ethics Approval: Not applicable.

Conflicts of Interest: The authors declare no conflicts of interest to report regarding the present study.

Supplementary Materials: The supplementary material is available online at https://doi.org/10.32604/jrm.2025.02024-0023.

References

1. Ncube LK, Ude AU, Ogunmuyiwa EN, Zulkifli R, Beas IN. An overview of plasticwaste generation and management in food packaging industries. Recycling. 2021;6:12. doi:10.3390/recycling6010012.
2. Waring RH, Harris RM, Mitchell SC. Plastic contamination of the food chain: a threat to human health? Maturitas. 2018;115:64–8. doi:10.1016/j.maturitas.2018.06.010.
3. Garc L, Cabrera-barjas G, Soria-hernandez CG, Castano J, Guadarrama-Lezama AY, Rodríguez-Llamazares S. Progress in starch-based materials for food packaging applications. Polysaccharides. 2023;3(1):136–77. doi:10.3390/polysaccharides3010007.
4. Cheng H, Chen L, McClements DJ, Yang T, Zhang Z, Ren F, et al. Starch-based biodegradable packaging materials: a review of their preparation, characterization and diverse applications in the food industry. Trends Food Sci Technol. 2021;114:70–82. doi:10.1016/j.tifs.2021.05.017.
5. Aslam A, Fawzy Z, Ahmed R, Riaz A, Nazir A. *Aloe vera* gel, an excellent base material for edible films and coatings. Trends Food Sci Technol. 2021;116:329–41. doi:10.1016/j.tifs.2021.07.035.
6. Tavassoli-Kafrani E, Shekarchizadeh H, Masoudpour-Behabadi M. Development of edible films and coatings from alginates and carrageenans. Carbohydr Polym. 2016;137:360–74. doi:10.1016/j.carbpol.2015.10.074.
7. Basumatary IB, Mukherjee A, Kumar S. Chitosan-based composite films containing eugenol nanoemulsion, ZnO nanoparticles and *Aloe vera* gel for active food packaging. Int J Biol Macromol. 2023;242:124826. doi:10.1016/j.ijbiomac.2023.124826.
8. Vianna TC, Marinho CO, Júnior LM, Ibrahim SA, Vieira RP. Essential oils as additives in active starch-based food packaging films: a review. Int J Biol Macromol. 2021;182:1803–19. doi:10.1016/j.ijbiomac.2021.05.170.
9. Liu D, Zhao P, Chen J, Yan Y, Wu Z. Recent advances and applications in starch for intelligent active food packaging: a review. Foods. 2022;11(18):2879. doi:10.3390/foods11182879.

10. Lauer MK, Smith RC. Recent advances in starch-based films toward food packaging applications: physicochemical, mechanical, and functional properties. Compr Rev Food Sci Food Saf. 2020;19:3031–83. doi:10.1111/1541-4337.12627.
11. Punia S, Scott W, Omodunbi A. Recent advances in thermoplastic starches for food packaging: a review. Food Packag Shelf Life. 2021;30:100743. doi:10.1016/j.fpsl.2021.100743.
12. Saxena A, Sharma L, Maity T. Enrichment of edible coatings and films with plant extracts or essential oils for the preservation of fruits and vegetables. Biopolym-Based Formul. 2020:859–80. doi:10.1016/B978-0-12-816897-4.00034-5.
13. Ramadas BK, Rhim J, Roy S. Recent progress of carrageenan-based composite films in active and intelligent food packaging applications. Polymers. 2024;16:1001. doi:10.3390/polym16071001.
14. Shahbazi M, Majzoobi M, Farahnaky A. Physical modification of starch by high-pressure homogenization for improving functional properties of κ-carrageenan/starch blend film. Food Hydrocoll. 2018;85:204–14. doi:10.1016/j.foodhyd.2018.07.017.
15. Thakur R, Saberi B, Pristijono P, Golding J, Stathopoulos C, Scarlett C, et al. Characterization of rice starch-ι-carrageenan biodegradable edible film. Effect of stearic acid on the film properties. Int J Biol Macromol. 2016;93:952–60. doi:10.1016/j.ijbiomac.2016.09.053.
16. Dmitrenko M, Kuzminova A, Cherian RM, Joshy KS, Pasquini D, John MJ, et al. Edible carrageenan films reinforced with starch and nanocellulose: development and characterization. Sustainability. 2023;15:15817. doi:10.3390/su152215817.
17. Ma X, Cheng Y, Qin X, Guo T, Deng J, Liu X. Hydrophilic modification of cellulose nanocrystals improves the physicochemical properties of cassava starch-based nanocomposite films. LWT. 2017;86:318–26. doi:10.1016/j.lwt.2017.08.012.
18. Pasquini D, de Morais LC, Costa PE. Nanofibers for environmental remediation. In: Nanotechnology for environmental remediation. Hoboken, NJ, USA: Wiley; 2022. p. 301–21.
19. Maan AA, Nazir A, Khan MKI, Ahmad T, Zia R, Murid M, et al. The therapeutic properties and applications of *Aloe vera*: a review. J Herb Med. 2018;12:1–10. doi:10.1016/j.hermed.2018.01.002.
20. Kumar S, Kalita S, Das A, Kumar P, Singh SB, Katiyar V, et al. *Aloe vera*: a contemporary overview on scope and prospects in food preservation and packaging. Prog Org Coat. 2022;166:106799. doi:10.1016/j.porgcoat.2022.106799.
21. Benítez S, Achaerandio I, Pujolà M, Sepulcre F. *Aloe vera* as an alternative to traditional edible coatings used in fresh-cut fruits: a case of study with kiwifruit slices. LWT-Food Sci Technol. 2015;61:184–93. doi:10.1016/j.lwt.2014.11.036.
22. Tong WY, Mohd Hashim NFF, Lim LS, Ring LC, Wen-Nee T. Antibacterial and antioxidant activities of ghee hiang sesame oil extract. Malays J Med Health Sci. 2023;19:75–81. doi:10.47836/mjmhs.
23. Onyeaka H, Obileke K, Makaka G, Nwokolo N. Current research and applications of starch-based biodegradable films for food packaging. Polymers. 2022;14:1126. doi:10.3390/polym14061126.
24. Oboulbiga EB, Douamba Z, Compaoré-Sérémé D, Semporé JN, Dabo R, Semde Z, et al. Physicochemical potential nutritional, antioxidant and health properties of sesame seed oil: a review. Front Nutr. 2023;10:1–13. doi:10.3389/fnut.2023.1127926.
25. Khezerlou A, Tavassoli M, Alizadeh-Sani M, Hashemi M, Ehsani A, Bangar SP. Multifunctional food packaging materials: lactoferrin loaded Cr-MOF in films-based gelatin/κ-carrageenan for food packaging applications. Int J Biol Macromol. 2023;251:126334. doi:10.1016/j.ijbiomac.2023.126334.
26. Khezerlou A, Tavassoli M, Sani MA, Ehsani A. Smart packaging for food spoilage assessment based on *Hibiscus sabdariffa* L. Anthocyanin-loaded chitosan films. J Compos Sci. 2023;7:404. doi:10.3390/jcs7100404.
27. Yang Z, Zou X, Li Z, Huang X, Zhai X, Zhang W, et al. Improved postharvest quality of cold stored blueberry by edible coating based on composite gum arabic/roselle extract. Food Bioprocess Technol. 2019;12:1537–47. doi:10.1007/s11947-019-02312-z.
28. Aydin G, Busra E. Characterisation and antibacterial properties of novel biodegradable films based on alginate and roselle (*Hibiscus sabdariffa* L.) extract. Waste Biomass Valorization. 2022;13:2991–3002. doi:10.1007/s12649-022-01710-3.

29. Nogueira GF, Fakhouri FM, de Oliveira RA. Extraction and characterization of arrowroot (*Maranta arundinaceae* L.) starch and its application in edible films. Carbohydr Polym. 2018;186:64–72. doi:10.1016/j.carbpol.2018.01.024.
30. Tuvikenea R, Truusa K, Vaherb M, Kailasb T, Martinc G, Kersen P. Extraction and quantification of hybrid carrageenans from the biomass of the red algae *Furcellaria lumbricalis* and *Coccotylus truncatus*. Proc Est Acad Sci Chem. 2006;55:40–53. doi:10.3176/chem.2006.1.04.
31. Silvério HA, Leite ARP, da Silva MDD, de Assunção RMN, Pero AC, Pasquini D. Poly(ethyl methacrylate) composites reinforced with modified and unmodified cellulose nanocrystals and its application as a denture resin. Polym Bull. 2022;79:2539–57. doi:10.1007/s00289-021-03621-0.
32. Chawalitsakunchai W, Dittanet P, Loykulnunt S, Tanpichai S, Prapainainar P. Extraction of nanocellulose from pineapple leaves by acid-hydrolysis and pressurized acid hydrolysis for reinforcement in natural rubber composites. IOP Conf Ser Mater Sci Eng. 2019;526:012019. doi:10.1088/1757-899X/526/1/012019.
33. Api AM, Belmonte F, Belsito D, Botelho D, Bruze M, Burton Jr GA, et al. RIFM fragrance ingredient safety assessment, myristic acid, CAS registry number 544-63-8. Food Chem Toxicol. 2019;130:110460. doi:10.1016/j.fct.2019.04.030.
34. Binks BP, Garvey EJ, Vieira J. Whipped oil stabilised by surfactant crystals. Chem Sci. 2016;7:2621–32. doi:10.1039/C6SC00046K.
35. de Oliveira M, Lima VMM, Yamashita SMA, Alves PS, Portella ACF. Experimental planning factorial: a brief review. Int J Adv Eng Res Sci. 2018;5:166–77. doi:10.22161/ijaers.5.6.28.
36. Redondo A, Mortensen N, Djeghdi K, Jang D, Ortuso RD, Weder C, et al. Comparing percolation and alignment of cellulose nanocrystals for the reinforcement of polyurethane nanocomposites. ACS Appl Mater Interfaces. 2022;14:7270–82. doi:10.1021/acsami.1c21656.
37. Kim J-H, Shim BS, Kim HS, Lee Y-J, Min S-K, Jang D, et al. Review of nanocellulose for sustainable future materials. Int J Precis Eng Manuf Technol. 2015;2(2):197–213. doi:10.1007/s40684-015-0024-9.
38. Nguyen HN, Dinh KD, Vu LTK. Carboxymethyl cellulose/*Aloe vera* gel edible films for food preservation. In: 5th International Conference on Green Technology and Sustainable Development (GTSD); 2020 Nov 27–28; Ho Chi Minh City, Vietnam. p. 203–8.
39. Anglès MN, Dufresne A. Plasticized starch/tunicin whiskers nanocomposite materials. 2. Mechanical behavior. Macromolecules. 2001;34:2921–31. doi:10.1021/ma001555h.
40. Di D, Civile I, Ambientale EE. Disintegration of different materials under simulated composting conditions in a laboratory-scale test [master's thesis]. Padua, Italia: University of Padova; 2022.
41. Tabasi RY, Ajji A. Selective degradation of biodegradable blends in simulated laboratory composting. Polym Degrad Stab. 2015;120:435–42. doi:10.1016/j.polymdegradstab.2015.07.020.
42. Chirayil CJ, Joy J, Mathew L, Mozetic M, Koetz J, Thomas S. Isolation and characterization of cellulose nanofibrils from *Helicteres isora* plant. Ind Crops Prod. 2014;59:27–34. doi:10.1016/j.indcrop.2014.04.020.
43. Wulandari WT, Rochliadi A, Arcana IM. Nanocellulose prepared by acid hydrolysis of isolated cellulose from sugarcane bagasse. IOP Conf Ser Mater Sci Eng. 2016;107:012045. doi:10.1088/1757-899X/107/1/012045.
44. Mak YW, Chuah LO, Ahmad R, Bhat R. Antioxidant and antibacterial activities of hibiscus (*Hibiscus rosa-sinensis* L.) and Cassia (*Senna bicapsularis* L.) flower extracts. J King Saud Univ—Sci. 2013;25:275–82. doi:10.1016/j.jksus.2012.12.003.
45. Othman M, Yusup AA, Zakaria N, Khalid K. Bio-polymer chitosan and corn starch with extract of hibiscus rosa-sinensis (hibiscus) as PH indicator for visually-smart food packaging. AIP Conf Proc. 2018;1985(1):050004. doi:10.1063/1.5047198.
46. Benalia A, Derbal K, Khalfaoui A, Pizzi A, Medjahdi G. The use of as natural coagulant in algerian drinking water treatment plant. J Renew Mater. 2022;10:625–37. doi:10.32604/jrm.2022.017848.
47. Subramonian W, Wu TY, Chai S-P. A comprehensive study on coagulant performance and floc characterization of natural Cassia obtusifolia seed gum in treatment of raw pulp and paper mill effluent. Ind Crops Prod. 2014;61:317–24. doi:10.1016/j.indcrop.2014.06.055.
48. Pop RM, Puia IC, Puia A, Chedea VS, Levai AM, Bocsan IC, et al. Pot *Aloe vera* gel—a natural source of antioxidants. Not Bot Horti Agrobot Cluj-Napoca. 2022;50:12732. doi:10.15835/nbha50212732.

49. Subando TR, Pranoto Y, Witasari LD. Optimization and characterization of arrowroot porous starch using thermostable α-amylase by response surface methodology. ResearchSquare. 2023;1–25. doi:10.21203/rs.3.rs-2440776/v1.
50. Zhao AQ, Yu L, Yang M, Wang C-J, Wang M-M, Bai X. Effects of the combination of freeze-thawing and enzymatic hydrolysis on the microstructure and physicochemical properties of porous corn starch. Food Hydrocoll. 2018;83:465–72. doi:10.1016/j.foodhyd.2018.04.041.
51. Damian KBBT, Bermundo KAC, Macatol YBL, Marino GPS, Aqoino RR. Fabrication and characterization of biocomposite membranes from polycaprolactone and native arrowroot (*Maranta arundinacea* L.). Extr Starch Mater Sci Forum. 2020;998:163–9. doi:10.4028/www.scientific.net/MSF.998.163.
52. Chakrabarty A, Teramoto Y. Recent advances in nanocellulose composites with polymers: a guide for choosing partners and how to incorporate them. Polymers. 2018;10:517. doi:10.3390/polym10050517.
53. Cheng C, Chen S, Su J, Zhu M, Zhou M, Chen T, et al. Recent advances in carrageenan-based films for food packaging applications. Front Nutr. 2022;9:1004588. doi:10.3389/fnut.2022.1004588.
54. Sabu Mathew S, Jaiswal AK, Jaiswal S. Carrageenan-based sustainable biomaterials for intelligent food packaging: a review. Carbohydr Polym. 2024;342:122267. doi:10.1016/j.carbpol.2024.122267.
55. Flores AC, Punzalan ER, Ambangan NG. Effects of Kappa-carrageenan on the physico-chemical properties of thermoplastic starch. KIMIKA. 2015;26:10–6. doi:10.26534/kimika.v26i1.10-16.
56. Giyatmi Melanie S, Fransiska D, Darmawan M, Irianto HE. Barrier and physical properties of arrowroot starch-carrageenan based biofilms. J Bio-Sci. 2018;25:45–56. doi:10.3329/jbs.v25i0.37498.
57. Wu Y, Liang Y, Mei C, Cai L, Nadda A, Le QV, et al. Advanced nanocellulose-based gas barrier materials: present status and prospects. Chemosphere. 2022;286:131891. doi:10.1016/j.chemosphere.2021.131891.
58. Liu R, Xuwang T, Wang Z, Zhang J, Lu P, Huang C. Water vapor barrier coating based on nanocellulose crystals stabilized AESO oil-in-water Pickering emulsion. Prog Org Coat. 2021;159:106479. doi:10.1016/j.porgcoat.2021.106479.
59. Shanmugam K, Doosthosseini H, Varanasi S, Garnier G, Batchelor W. Nanocellulose films as air and water vapour barriers: a recyclable and biodegradable alternative to polyolefin packaging. Sustain Mater Technol. 2019;22:e00115. doi:10.1016/j.susmat.2019.e00115.
60. Arribada RG, Behar-Cohen F, de Barros ALB, Silva-Cunha A. The use of polymer blends in the treatment of ocular diseases. Pharmaceutics. 2022;14:1431. doi:10.3390/pharmaceutics14071431.
61. del Campo A, de Lucas-Gil E, Rubio-Marcos F, Arrieta MP, Fernández-García M, Fernández JA, et al. Accelerated disintegration of compostable Ecovio polymer by using ZnO particles as filler. Polym Degrad Stab. 2021;185:109501. doi:10.1016/j.polymdegradstab.2021.109501.
62. Arrieta MP, López J, Rayón E, Jimenez A. Disintegrability under composting conditions of plasticized PLA-PHB blends. Polym Degrad Stab. 2014;108:307–18. doi:10.1016/j.polymdegradstab.2014.01.034.